

Assessing the pollutant evolution mechanisms of heavy pollution episodes in the Yangtze-Huaihe valley: A multiscale perspective

Wenxing Jia ^{a,b}, Xiaoye Zhang ^{a,c,*}, Yaqiang Wang ^a

^a Key Laboratory of Atmospheric Chemistry of CMA, Chinese Academy of Meteorological Sciences, Beijing, 100081, China

^b Key Laboratory for Aerosol-Cloud-Precipitation of China Meteorological Administration, Nanjing University of Information Science & Technology, Nanjing, 210044, China

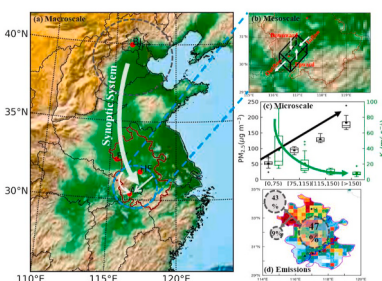
^c Center for Excellence in Regional Atmospheric Environment, IUE, Chinese Academy of Sciences, Xiamen, 361021, China



HIGHLIGHTS

- Heavy pollution episodes were mainly controlled by synoptic system in the Yangtze-Huaihe.
- Residual layer transport mechanism on aerosol pollution was demonstrated.
- The relationship between turbulence characteristics and aerosol pollution was studied.
- The contributions of regional transport and local emissions are equally important for the Yangtze-Huaihe.

GRAPHICAL ABSTRACT



ARTICLE INFO

Keywords:

Yangtze-Huaihe region
Transport and cumulative stages
Residual layer
Turbulent characteristics
Contribution of emissions

ABSTRACT

The Yangtze-Huaihe (YH) region experiences heavy aerosol pollution, characterized by high PM_{2.5} concentration. To unravel the pollutant evolution mechanism during the heavy pollution episodes (HPEs), this study combined observational data analysis and three-dimensional WRF-Chem simulations. From December 2, 2016 to January 15, 2017, YH region experienced 4 HPEs under the control by synoptic system, normally associated with a transport stage (TS) and a cumulative stage (CS). During the TS, pollutants are transported to the north of YH region through the near-surface, and then transported to the “mountain corridor” through the residual layer (RL) under the influence of prevailing wind. For the RL transport mechanism, the change of pollutant concentration cannot only consider the net flux in the horizontal direction, but also the role of the vertical movement is extremely important and cannot be ignored. By analyzing the mass conservation equation of pollutant, the results show that the advection transport and turbulent diffusion have a synergistic effect on the change of pollutant in the CS of three HPEs. The change of turbulence characteristics also affected by topography. For the “mountain corridors”, which is accompanied by variable wind direction and turbulence diffusion is easily affected by wind shear. In addition, the turbulence characteristics are different during the TS and CS, especially the strong stable conditions in the CS at nighttime. The turbulence is intermittent, and the model has insufficient performance for turbulence, which will lead to differences for the simulation of pollutant concentration. In short, as the PM_{2.5} concentration linearly increases, the friction velocity (turbulent diffusion coefficient) decreases 63% (80%), 61% (78%) and 45% (68%), respectively. Therefore, the change of pollutants is less sensitive to the change of turbulence during the HPEs. The contribution of regional transport (local emissions) reaches 43% (47%), thus we

* Corresponding author. Key Laboratory of Atmospheric Chemistry of CMA, Chinese Academy of Meteorological Sciences, Beijing, 100081, China.
E-mail address: xiaoye@cma.gov.cn (X. Zhang).

need pay attention to the contribution of each part during the HPEs, which will help us to build a certain foundation for the emission reduction work in the future.

1. Introduction

China has witnessed continual episodes of heavy haze pollution in recent years. Accompanying unfavorable meteorological conditions include stronger stable stratification, lower wind speed, higher relative humidity and shallower planetary boundary layer height (PBLH), which lead to the explosive growth of PM_{2.5} (Miao et al., 2018b; Zhang et al., 2015; Zhong et al., 2018). Due to the prosperous economic growth and intensive urban expansion, heavy aerosol pollution events have frequently occurred in Anhui, characterized by high PM_{2.5} concentrations (Deng et al., 2012, 2015; Shi et al., 2018a, b; Wang et al., 2014b). Anhui, the hinterland of Yangtze-Huaihe (YH) valley, is located in eastern China (Fig. 1a), which is surrounded by the Dabie Mountains in the west and the Huangshan Mountains in the south, with a north-to-south span of ~570 km and an east-to-west span of 450 km. The altitude of the western mountains is ~1770 m, and the altitude of the

southern mountains is ~1800 m. The physical evolution mechanism of pollutants will be affected by topography (Ning et al., 2019; Zhang et al., 2019a). Both Deng et al. (2012) and Shi et al. (2018a) used the HYSPLIT model to reveal the aerosol characteristics and their relationships with meteorological conditions in Anhui. Shi et al. (2018a) demonstrated that Anhui was affected by two main groups of shorter trajectories from northeast and northwest, while Deng et al. (2012) used an Angstrom exponent to distinguish contributions of different sources. Based on long-term meteorological data from 1980 to 2015, Shi et al. (2018b) showed that regional haze usually corresponded to high humidity and small wind speed, and the regional aerosol optical depth (AOD) was around 2.3 times of that of clear day.

The high aerosol pollutant concentrations occurred mainly within the planetary boundary layer (PBL), which is the portion of the lower troposphere directly influenced by the Earth's surface (Stull, 1988). On a local scale, the exchange of aerosol pollutants within the PBL through

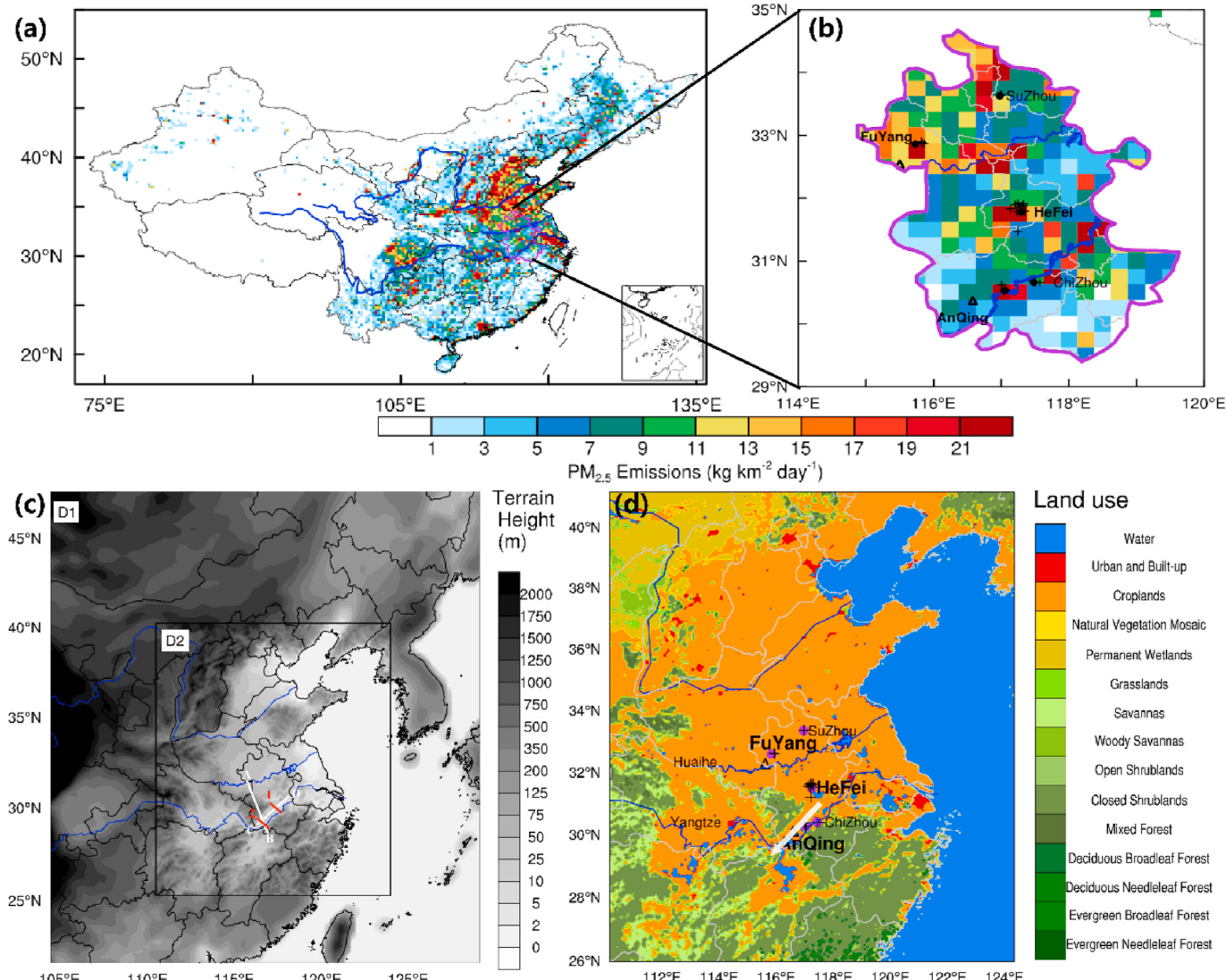


Fig. 1. The emission rate of PM_{2.5} in December 2016 (a) in China and (b) in Anhui. (c) Map of the model domain and terrain height (m AGL), the white solid lines AB (CD) and red solid lines 1 (2) denote the locations of vertical cross sections shown in Figs. 5 and 6c, d. (d) Land use categories in domain 2, and the location of the “mountain corridor” is indicated by a white shaded arrow. The locations of the surface meteorological stations and air quality monitoring sites in Anhui are marked by purple dots and black pluses, respectively. The locations of the sounding sites are denoted by black triangles in (d).

intricate processes/structures associated with turbulent eddies when source emissions are unchanged for a short period (Li et al., 2017). Therefore, the strength of thermal stratification (e.g., anomalous temperature inversion) and intensity of mechanical turbulent (e.g., wind fields) determine the dispersion and transportation of aerosol pollutants within the PBL (Stull, 1988). Specifically, turbulent motion (i.e., dynamic and thermodynamic) determines the variability of meteorological parameters within the PBL, and consequently affects the change of pollutant concentration. In turn, the change of pollutants also affects the variation of PBL structure (Ding et al., 2016a; Ma et al., 2020), and even turbulence (Wilcox et al., 2016) by radiation feedback. In addition, the PBL height (PBLH) also plays a vital role. It is commonly used to characterize the vertical extent of pollutants mixing within PBL (Miao et al., 2018b; Seidel et al., 2010). The aerosol pollutants are not only influenced by PBL structures, but also by large-scale synoptic patterns (Miao et al., 2019). On a large-scale, the synoptic patterns affect the day-to-day variations and regional linkage of aerosol pollutants (Miao et al., 2019; Yang et al., 2018). Besides, the pollution events are primarily caused by the high emissions that are contributed by the agriculture, transport, residential, industry and power (Huang et al., 2018; Zhang et al., 2015). Hefei is the capital of Anhui Province, which is influenced by both natural and anthropogenic aerosols (e.g., smoke) from the burning of agricultural residues (Wang et al., 2014b). Thereby, emissions are also play an important role for the pollution events.

To date, great efforts have been devoted to investigating the pollution issues in several highly polluted regions, including the North China Plain (NCP) (Ye et al., 2016; Zheng et al., 2019; Zhong et al., 2017, 2018), Yangtze River Delta (YRD) (Ding et al., 2016b; Zhong et al., 2019b), Pearl River Delta (PRD) (Lo et al., 2006; Wu et al., 2013; Zhong et al., 2019b), Northeast China (NEC) (Li et al., 2018; Miao et al., 2018a), Sichuan Basin (SCB) (Liao et al., 2018; Ning et al., 2018; Zhang et al., 2019a) and Central China (CTC) (Liu et al., 2018; Zhong et al., 2019b). And only few studies devoted to investigate the aerosol optical properties, spatial-temporal distribution characteristics and case study in Anhui (Deng et al., 2012, 2015; Shi et al., 2018a, b). The complexity of PM_{2.5} pollution lies in the variety and interdependence of atmospheric processes acting on different scales (e.g., the specific synoptic system-macroscale, evolution of PBL structures-mesoscale and turbulence changes-microscale) in Anhui of YH region (i.e., especially during the heavy pollution episodes (HPEs)), however, which is yet to be well understood.

The annual average concentrations of PM_{2.5} is 86 ± 59 µg/m³ during 2013 in Hefei, which is similar to Beijing (87 ± 67 µg/m³) and greater than the limit of Chinese Ambient Air Quality Standard (i.e., 35 µg/m³) (Wang et al., 2014a). Since the promulgated of the Air Pollution Prevention and Control Action Plan (the Action Plan), aerosol pollution issues and PM_{2.5} concentrations have been effectively controlled and reduced (Zhang et al., 2019b; Zhang et al., 2019c). The annual average concentrations of PM_{2.5} has dropped to 57 ± 38 µg/m³ in Hefei until 2016. However, the average concentrations of PM_{2.5} is also as high as 84 ± 44 µg/m³ during winter in 2016. Therefore, the pollution situation still has not been improved significantly during winter in Anhui. This study comprehensively analyzes the pollution situation in the YH region from the perspective of multiscale atmospheric, especially during the HPEs. Firstly, the influence of large-scale synoptic system on the YH region is verified, especially connection with the Beijing-Tianjin-Hebei (BTH) region. Secondly, we are able to figure out the role of PBL structure on the evolution of pollution and present an important aerosol transport mechanism. Finally, the variation of turbulence characteristics is quantitatively analyzed during the HPEs by simulation results. Moreover, the contributions of local emissions (i.e., local emissions in Anhui) and regional transport (i.e., trans-boundary transport from emissions outside Anhui (no-Anhui) to local (Anhui)) are calculated in the different stages of HPEs.

2. Data and methodology

2.1. Data

In this study, the aerosol pollution level in Anhui is denoted by near-surface hourly PM_{2.5} concentration, collecting from five major cities (23 air quality monitoring sites), including Fuyang, Suzhou, Hefei, Anqing and Chizhou from December 2, 2016 to January 15, 2017 (marked by the black pluses in Fig. 1d). At each monitoring site, the hourly PM_{2.5} concentration is measured using the micro oscillating balance method (Tapered Element Oscillating Microbalance, TEOM) and/or the β absorption method (Beta Attenuation Monitor, BAM) (Zhao et al., 2016). The uncertainty of PM_{2.5} concentration is less than 5 µg/m³. Besides, the hourly ground-level meteorological variables are obtained from five automatic weather stations (AWSs) in Anhui (marked by the purple dots in Fig. 1d), including the hourly temperature, relative humidity, wind speed and direction.

In addition to investigate the linkages between the PBL structures and aerosol pollution during the HPEs, the radiosonde measurements collected from the Fuyang site (32.54 °N, 115.5 °E, 31 m above sea level) and the Anqing site (30.37 °N, 116.58 °E, 62 m above sea level) (marked by the black triangles in Fig. 1d) from December 2, 2016 to January 15, 2017 are analyzed. These two stations are equipped with L-band radiosonde systems (Guo et al., 2016), which provide fine resolution (1 Hz) profiles of temperature, humidity and wind twice a day at 0800 and 2000 local time (LT). As the previous studies reported (Bian et al., 2011; Zhang et al., 2018), the accuracy of the temperature within the lower BL is similar to that of GPS RS 92 radiosonde (Vaisala, USA), which is less than 0.1K. Thus, the data of L-band radiosonde systems are good enough to investigate the PBL structures.

Finally, as the previous studies pointed out, the high concentration of PM_{2.5} is associated with low PBLH during HPEs in wintertime (Miao et al., 2018b, 2019; Zhong et al., 2018, 2019b). Therefore, the PBLH represents the atmospheric environmental capacity, which is estimated by the bulk Richardson number (Ri) method (Seidel et al., 2012; Vogelezang and Holtslag, 1996). The Ri is defines as the ratio of turbulence associated with buoyancy to the turbulence caused by mechanical shear, which is expressed as Equation S(1) (i.e., Eq. (S1)). It is a dimensionless and the PBLH is estimated as the lowest level at which the interpolated Ri crossed the critical value of 0.25. The definition of PBLH in the ACM2 PBL scheme also using the Richardson number method (Jia and Zhang, 2020). Although this method can be used for both convective and stable conditions, the PBLH of stable stratifications is not the actual height of surface inversion layer (i.e., the height of surface inversion layer is defined as the height of the stable boundary layer at night) (Seidel et al., 2010; Yamada, 1976). Though this method has two problems: (1) Ri is sensitive to the data vertical resolution and (2) it is affected by the earth's rotation, the Brunt-Vaisala frequency and surface roughness (Zhang et al., 2020), this method has been widely utilized by the observational studies in China (Guo et al., 2016; Miao et al., 2018b), United States and Europe (Seidel et al., 2012).

2.2. Three-dimensional meteorology-chemistry simulations

To better understand the variation of turbulence characteristics within the PBL and the transport mechanism of pollutant between Yangtze-Huaihe (YH) and Beijing-Tianjin-Hebei (BTH) regions during the HPEs, three-dimensional simulations are enforced using the Weather Research and Forecasting model coupled with Chemistry (WRF-Chem version 3.9.1) (Grell et al., 2005) from December 2, 2016 to January 15, 2017. To reduce the systematic model errors, 91-h simulation is conducted beginning from 0000UTC of three days ago for each day. The first 64-h of each simulation is considered as the spin-up period, the next 24-h is used for further analysis and the remaining 3-h is discarded (e.g., run one simulation from November 29, 0000 UTC (0800 BJT) to December 02, 1800 UTC (December 03, 0200 BJT), and for total 91 h.

We need the results from the December 02, 0000 BJT to 2300 BJT. From November 29, 0800 BJT to December 01, 2300 BJT is considered as the spin-up period (in total 64-h), and the results from December 03, 0000 BJT to 0200 BJT is discarded). The initial and boundary conditions are set up using the National Centers for Environmental Prediction (NCEP) global final (FNL) reanalysis data. The FNL reanalysis fields are based on the 6 h temporal resolution (i.e., 00:00 (08:00), 06:00 (14:00), 12:00 (18:00), 18:00 (02:00) UTC (BJT)) by the Global Data Assimilation System with a resolution of $1^\circ \times 1^\circ$ (<https://rda.ucar.edu/datasets/ds083.2/>). And the chemical initial and boundary conditions are set using the global output of Model for Ozone and Related chemical Tracers (MOZART) (<http://www.acm.ucar.edu/wrf-chem/mozart.shtml>). In the horizontal direction, two nested domains with horizontal resolutions of 33 and 6.6 km are used (Fig. 1c). In the vertical direction, 48 layers are set that from the surface to the 50 hPa level, with 21 layers below 2 km (AGL) to refined processes resolving within PBL.

The physics parameterization schemes selected for this study included the Second generation of Asymmetric Convective Model (ACM2) PBL scheme (Pleim, 2007), Noah land surface scheme (Chen and Dudhia, 2001), single layer urban canopy model (UCM) (Kusaka et al., 2001), Lin microphysics scheme (Lin et al., 1983), RRTMG long-wave/shortwave radiation scheme (Iacono et al., 2008) and Grell-3 cumulus scheme (Grell and Devenyi, 2002). The chemical mechanism used in this simulation is the RADM2-MADE/SORGM scheme (Ackermann et al., 1998; Schell et al., 2001).

The anthropogenic emissions of BC, CO, NH₃, NO_x, PM_{2.5}, PM₁₀, OC and volatile organic compounds (VOCs) are set based on the monthly Multi-resolution Emission inventory for China (MEIC) of 2016 provided by Tsinghua University, with a resolution of $0.25^\circ \times 0.25^\circ$. The spatial distribution of PM_{2.5} emissions is shown in Fig. 1b, and indicates that the emissions in Anhui. As seen in Table S1, the rate of the direct emissions of primary fine particles of PM_{2.5} reaches 44256 Mg/month in Anhui and other main secondary fine particles precursors (SO₂, NO_x, NH₃, VOCs) are also higher. It is well known that the formation of the secondary aerosol pollutant is a complicated nonlinear process. Nevertheless, it is difficult straightforward to isolate the contributions from different factors in a nonlinear process (Streets et al., 2007; Wu et al., 2017). Thus, the factor separation approach (FSA) can be used in this study to separate the effect of one single factor, which has been widely used to evaluate source effects (Carnevale et al., 2010; Gabusi et al., 2008). To evaluate the contributions of local emissions (L) and regional transport (T), so there are three sensitivity experiments and one basic experiment are set using the zero-out method (Table 1) (Streets et al., 2007). The contribution of local emissions is expressed as the results of EXP_L minus EXP₀ (i.e., $E'_L = E_L - E_0$, and the E_0 is the background concentration), and the contribution of region transport is denoted by the results of EXP_T minus EXP₀ (i.e., $E'_T = E_T - E_0$). Besides, the synergistic interaction is estimated by basic experiment (EXP_{LT}) minus the sum of contributions of local emission (EXP_L-EXP₀), region transport (EXP_T-EXP₀) and background concentration (EXP₀) (i.e., $E'_{LT} = E_{LT} - (E'_L + E'_T + E_0)$).

3. Results and discussion

In this section, the simulation results are evaluated against the observations, and the pollution characteristics in YH region are presented. Then, the role of synoptic systems, the evolution of PBL structure, and

Table 1
Experimental design.

Experiment description	Emission description
EXP _{LT}	With emission in the whole domain
EXP _L	Only emission in the Anhui Province
EXP _T	Without emission in the Anhui Province
EXP ₀	Without emission in the whole domain

the variation of the turbulence characteristics during the HPEs in the YH region are proved one by one. Finally, the contribution of emission sources is calculated and testified.

3.1. Validation of simulation results

To better evaluate the model performance, Fig. S1 shows the Taylor diagram of various parameters (i.e., include hourly 2 m temperature (T₂), hourly 2 m relative humidity (RH₂), hourly 10 m wind speed and direction (WS₁₀ and WD₁₀), hourly and daily PM_{2.5} concentration, and PBLH). Good agreement is found between simulated and observed T₂, with a high index of agreement (IOA) of 0.93–0.95, an approximately 1 of normalized standardized deviations (NSTD) of 1.00–1.10 and an extremely small relative bias (RB) of $-0.05\% \sim 0.15\%$. The simulated RH₂ also agrees well with the observed (IOA = 0.76–0.90, NSTD = 0.96–1.16, RB = $-0.46\% \sim -14.1\%$). As to the simulated WS₁₀, the model results tend to overestimate the wind speed to varying degrees (RB = $47.0\% \sim 108.4\%$), which is the common problem and a disadvantage of model (Jimenez and Dudhia, 2012). And the change of wind direction for most cities is well reproduced, but is poorly simulated in Anqing. Because Anqing is located in the “mountain corridor” between Dabie Mountains and Huang Mountains (Fig. 1d), thus the terrain disturbs the wind direction. With respect to the PM_{2.5} concentration, the model also reproduces the observation results (IOA = 0.68–0.75, NSTD = 0.96–1.32, RB = $-0.42\% \sim 8.79\%$). Despite these discrepancies, good agreement can be found between the observed and simulated daily average PM_{2.5} concentration as shown in Fig. S2 (IOA = 0.82–0.86).

Besides, the simulated and observed profiles of temperature, relative humidity and wind speed and direction present a good consistency (not shown). Meanwhile, the simulated and observed PBLH also are in good agreement at 0800 and 2000 (BJT) in Fuyang (IOA = 0.80) and Anqing (IOA = 0.70) (not shown). As a whole, the simulated near-surface parameters (i.e., T₂, RH₂, WS₁₀, WD₁₀ and PM_{2.5}), vertical meteorological parameters (i.e., T, RH, WS and WD) and PBLH display reasonably well consistency with the observations, which afford a sound basis to use the simulated results to demonstrate the physical processes within the PBL.

3.2. Overview of the heavy pollution episodes

Several heavy pollution episodes occurred in the YH region from December 2, 2016 to January 15, 2017. According to the hourly PM_{2.5} concentration, the heavy pollution period is defined when the maximum daily PM_{2.5} concentration is greater than $100 \mu\text{g m}^{-3}$ for 3 days (Zhong et al., 2019a). Fig. 2a shows the temporal evolution of PM_{2.5} concentrations and PBLH from December 2, 2016 to January 15, 2017 in Fuyang. It is found that there are four HPEs occur with each lasting for 5–8 days. In Fig. 2, the early periods of HPEs are briefly referred to as the transport stage (TS), the prevailing wind is northerly and wind speed is larger (Fig. 2d). The PBLH increases with increasing PM_{2.5} concentration during the TS (Fig. 2a). To the later periods of HPEs, the corresponding stage is cumulative stage (CS), which is accompanied by the stable atmospheric stratification (i.e., anomalous temperature inversion ($\Delta T = \sim 3\text{K}$)), static wind ($< 1 \text{ m s}^{-1}$) and higher relative humidity (70%–80%) in the lower atmosphere (Fig. 2b–d), indicating that the near-surface circulation is beneficial to accumulate aerosol pollutants. As seen in Fig. S3, there are also four HPEs and two stages in Anqing. The difference between two cities (Fuyang and Anqing) is mainly reflected in the process of HPE4. During the HPE4, Anqing experienced a longer transport process than that of Fuyang (96 h vs 42 h; Figs. 2d and S3d). Due to the influence of terrain, either stronger northeasterly wind or static wind below 1 km in Anqing (Fig. S3d).

For HPE1 process, the daily mean PM_{2.5} concentration increases from 77.5 to $163.7 \mu\text{g m}^{-3}$ in Fuyang, and the decreasing PBLH (from 362.1 to 169.5 m) can compress pollutants into a shallow layer (Fig. 3a). During the HPE2 and HPE3, the PBLH reduced to below 100 m, when the daily mean PM_{2.5} concentration explosively grew to $\sim 300 \mu\text{g m}^{-3}$

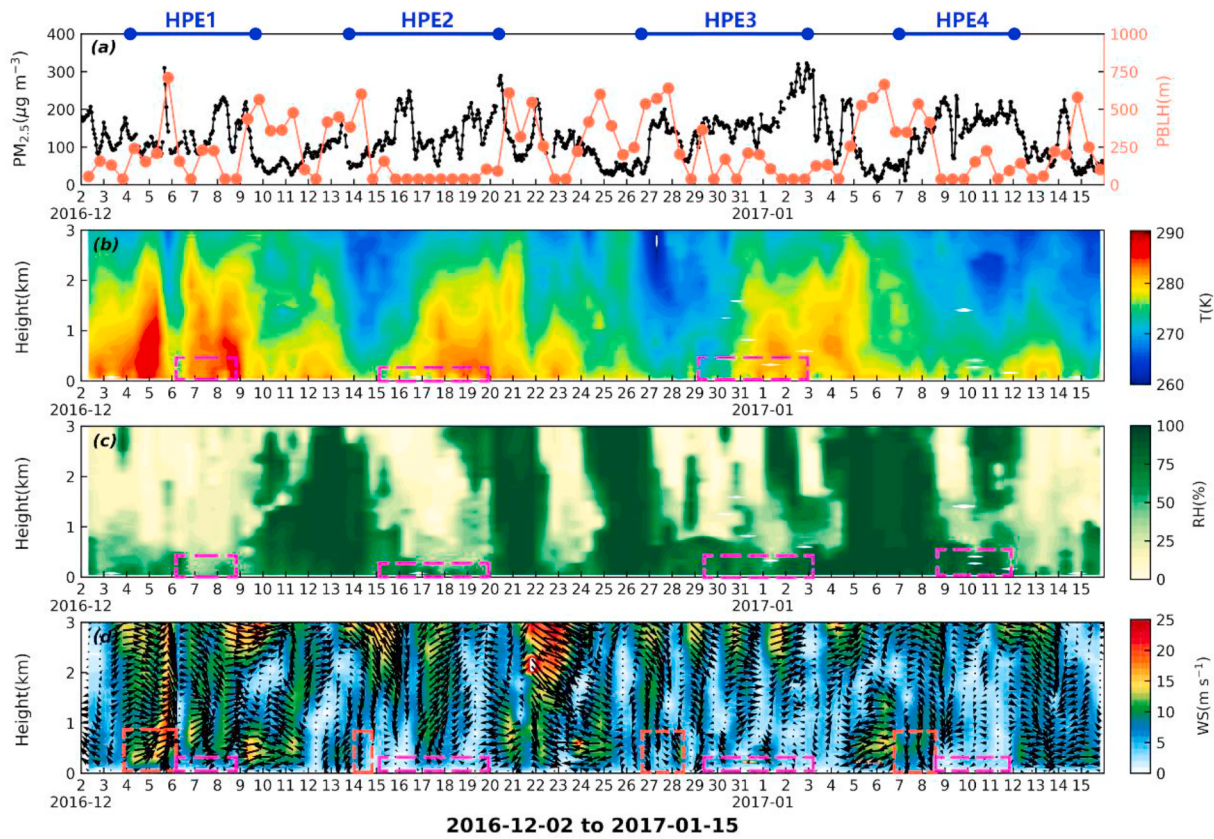


Fig. 2. Time series of (a) observed hourly PM_{2.5} concentration and PBLH. Time-height cross sections of (b) temperature, (c) relative humidity, and (d) wind speed and direction derived from sounding data in Fuyang.

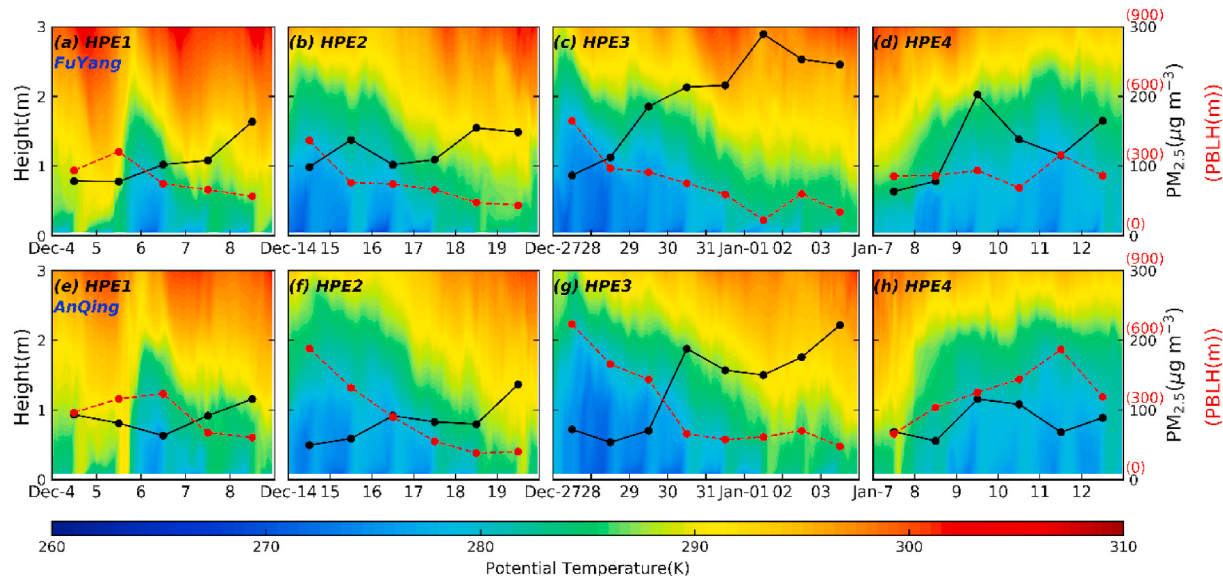


Fig. 3. Time series of daily mean PM_{2.5} concentration, PBLH and time-height cross sections of potential temperature from the simulation results in the HPE1-4 in (a-d) Fuyang and (e-h) Anqing.

(Fig. 3b, c, f, g). Meanwhile, the boundary layer becomes more stable compared with that of HPE1. During the HPE4, the PBLH continuously increases with increasing the PM_{2.5} concentration in Anqing, because of the longer TS (Fig. 3h). The temperature inversion in the CS is significantly stronger than that of the TS (Figs. 2b and S3b). Fig. S4 shows the position and thickness of the temperature inversion, and the thickness of the temperature inversion is described as $z_2 - z_1$ when $\Delta T > 0$. The surface

inversion in Fuyang is stronger than that in Anqing at nighttime (Fig. S4), which is more favorable for pollutant accumulation. During the most cumulative stages, strong inversion occurred with calm winds, which indicate that the horizontal movement of air mass is not obvious, so the contribution of topography to this inversion is limited.

3.3. Role of the synoptic system-macroscale

Recently, Huang et al. (2020b) found the long-range transport of pollutants between YRD and NCP, and indicated that the fast advection of aged regional plumes by cold fronts from the NCP to YRD region. However, under the evolution of the synoptic system, what are the similarities and differences in the pollution situation of these two regions? Fig. S5 shows the time series of PM_{2.5} concentration in YH region with four HPEs and Beijing-Tianjin-Hebei (BTH) region with three HPEs (Zhong et al., 2018). The PM_{2.5} concentration dropped sharply in the BTH region, which began to rise in the YH region during the initial stage of HPE1. The PM_{2.5} concentration decreases first during the later stage of HPE1 in the BTH region (Fig. S5). For the HPE2 and HPE3, the PM_{2.5} concentration increases almost simultaneously in the YH and BTH regions, and decreases earlier in the YH region (Fig. S5). The PM_{2.5} concentration began to rise during the HPE4 in the YH region, which is undergoing the dissipative stage of HPE3 in the BTH region (Fig. S5). The spatial distributions of PM_{2.5} concentration and wind vectors presented in Fig. 4. At the beginning of the TS, the aerosol pollutants are transported to the YH region and other places from the BTH region under the influence of northerly winds (Fig. 4a-d; Fig. S6). During the TS, a radial geopotential filed at 500-hPa over China and a surface high pressure lay northwest of the BTH region, which northerly winds carrying the polluted air from the BTH region to the YH region (Fig. S6; Fig. S7a). Then with the synoptic situation changed, the PM_{2.5} concentration of these two regions increases simultaneously (Fig. S5; Fig. 4f and g). Under the control of 500-hPa straight westerly air flow and the uniform pressure field (Fig. S7b), and local pollutants begin to accumulate during the CS. For the dissipative stage, the pollutant concentration decreases first in the YH region (Fig. S5), because of the stronger pressure gradient (Fig. S7c). The easterly wind from the Yellow Sea cannot affect the BTH region and the uniform pressure field in the BTH region (Fig. S7c), results in the pollutant concentration not decreasing simultaneously in these two regions (Fig. S5). When the easterly wind gradually changes to the northeasterly, the stronger cold air mass can put away pollutants in the BTH region. When the pollutant

concentration decreases in the BTH region, it may be accompanied by the initial formation of the next HPE in the YH region (e.g., HPE3 and HPE4 in the YH region, only HPE3 in BTH region) (Fig. S5; Fig. 4d, h).

3.4. Evolution of PBL structure-mesoscale

As mentioned above, pollution situation in the YH region is influenced by the BTH region under the influence of macroscale synoptic background. When pollutants are transported from BTH to YH region, the pollutant concentration is different in the different places of YH region. What effect does the change of PBL structure have on the evolution of pollutant concentration? We select three TSs in the HPE1-3 and mainly analysis the results of HPE1 (i.e., December 5, 2016) in the YH region. Under the strong northwesterly wind condition, the aerosol pollutants of YH region increase explosively (Figs. 2a and S3a). When the northwesterly wind prevailed, the first explosive growth phase occurred in the north of Anhui (e.g., Fuyang), and about 5 h later, the phenomenon of explosive growth happened in the south of Anhui (e.g., Anqing) (Figs. 2a and S3a). The reason of the difference in explosive growth time between the north and south is not just the distance of north-south. Aerosol pollutants are transported from the north of Anhui to Fuyang at 14:00 (Fig. 5a), and then continued to transport to the southward. The pollutants reached the Dabie Mountains at 18:00 (Fig. 5b), some pollutants crossed the mountains to reach Anqing, and other pollutants bypassed the mountains and transported to the southward (not shown). Then, the wind direction changes to northeasterly, the concentration of pollutants began to increase at 19:00 in Anqing (Fig. 5c and d). At the same time, a large amount of pollutants is transported to Chizhou and Anqing under the influence of northeasterly wind, which result in explosive growth events in Anqing. If the northwesterly wind not change the direction, the PM_{2.5} concentrations will continue to increase in the north of Anhui, and will not induce explosive growth events in Anqing (e.g., December 22, 2016, Figs. 2a and S3a). Accordingly, the influence of topography and prevailing winds first caused the difference in pollution levels between the north and south of the YH region.

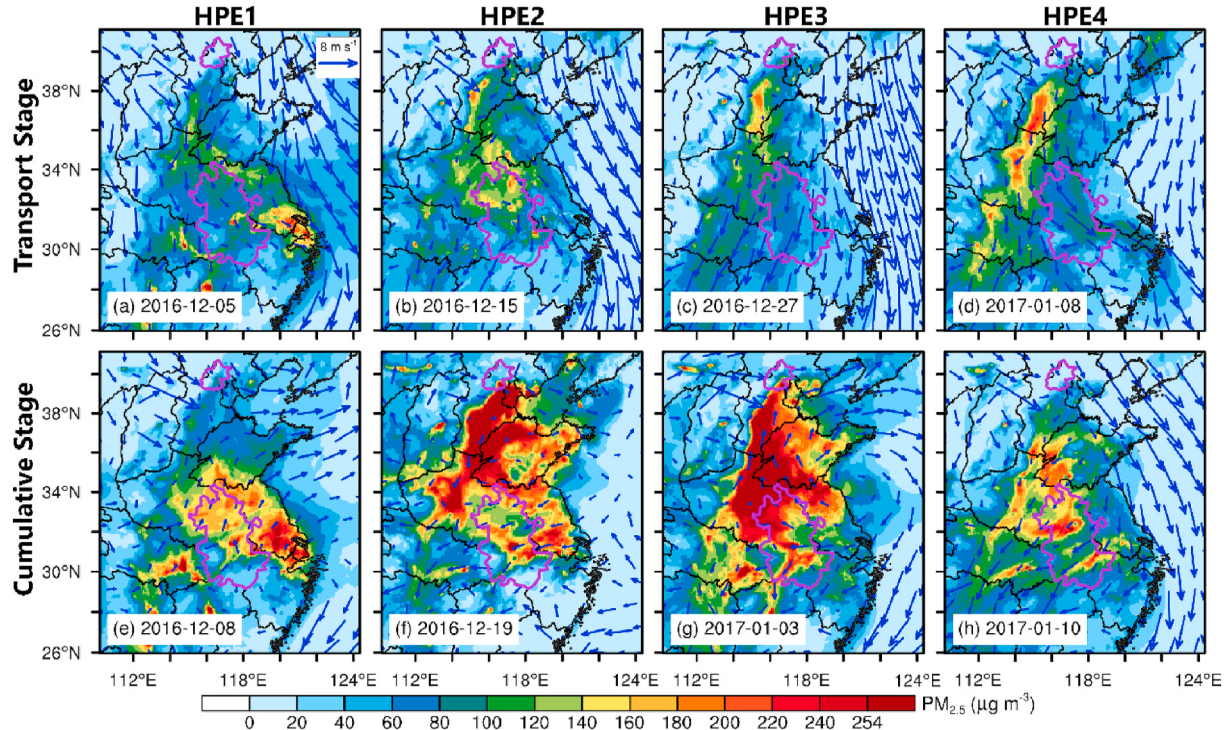


Fig. 4. Spatial distributions of simulated near-surface daily PM_{2.5} concentration (shaded) and wind vectors (arrow) in the transport and cumulative stages during 4 HPEs.

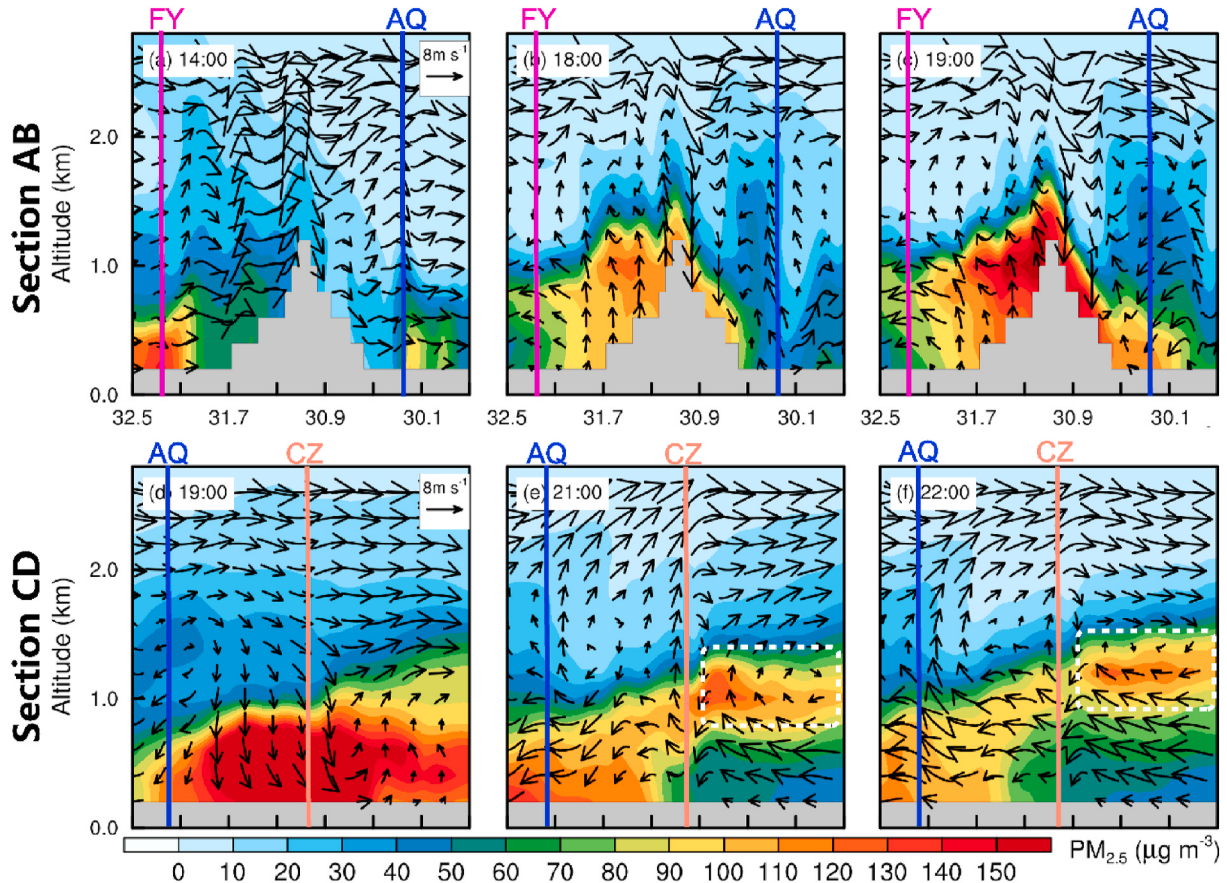


Fig. 5. Vertical cross sections AB (CD) of simulated $\text{PM}_{2.5}$ concentration at (a) 14:00, (b) 18:00 and (c) 19:00 ((d) 19:00, (e) 21:00 and (f) 22:00) on December 5, 2016, overlaid with the wind vector fields. Note that the vertical velocity is multiplied by a factor of 20 when plotting the wind vectors, and the approximate locations of Fuyang (FY), Anqing (AQ) and Chizhou (CZ) are indicated using the purple, blue and orange lines (texts). The locations of the cross sections are marked by the white lines in Fig. 1c. (For interpretation of the references to color in this figure legend, the reader is referred to the Web version of this article.)

Although the simulated wind speed is larger and the trend of the sudden change of pollutant concentration is offset, the transport process is well presented. After sunset, the part above the top of PBL is the residual part of the mixing layer during the daytime, that is, residual layer (i.e., RL) (Stull, 1988: Fig.1.7). The low-level wind direction gradually turned to the northeasterly wind at 19:00, pollutants transported from the northeast of Anqing along the “mountain corridor” to the Anqing (Fig. 5c and d). In the transport process, the mechanism of pollutant transport is different from that of early periods (i.e., pollutants transported to Fuyang). In the early periods, the pollutants transported to Fuyang in the low-level atmosphere (Fig. 5a). After, some pollutants are transported to the above the local area through the RL, and then reached the near-surface under the action of subsidence airflow (Fig. 5e). The $\text{PM}_{2.5}$ flux transported downward to the ground reaches $0.018 \text{ kg s}^{-1} \text{ km}^{-2}$ (Fig. 6a). After 22:00, as the dominant role of northeasterly wind strengthened, the pollutants gradually transported to downwind region (Fig. 5f). Meanwhile, the pollutants of RL continued to transport to downwind region without the effect of subsidence airflow (Fig. 5f). With the updraft dominates, the pollutants will be transported upward to RL, but not break through the top of the RL ($\sim 1200 \text{ m}$), the $\text{PM}_{2.5}$ transport flux reaches $0.012 \text{ kg s}^{-1} \text{ km}^{-2}$ (Fig. 6a). HPE2 and 3 also have a similar mechanism to HPE1 during the TS (not shown). To sum up, there is a vital pollutant transport mechanism in the TS, that is, the residual layer transport mechanism.

In the horizontal direction, from the 1800 to 2300, the $\text{PM}_{2.5}$ flux through cross section 1 (2) is from 16.5 (-2) to -11.5 (-23.8) kg s^{-1} within the PBL. The pollutant concentration not increases explosively because the subsidence airflow is weaker (Fig. 6a), PBLH is higher and

stronger horizontal transport (Fig. 6c) at the 1800. At 1900, the vertical (horizontal) movement begin to strengthen (weaken) (Fig. 6a and c), the PBLH decreases continuously and the pollutant concentration increases gradually. The vertical velocity (w) reaches maximum (-0.16 m s^{-1}) (Fig. 6a) and the horizontal velocity (u) on the cross section 1 changes to negative value at 2000, the pollutant concentration increases further (Fig. 6c). Although the absolute value of horizontal velocity (u) on the cross section 2 and $\text{PM}_{2.5}$ flux increases simultaneously (Fig. 6d), the increase rate of $\text{PM}_{2.5}$ flux on the cross section 1 ($18 \text{ kg s}^{-1}/2\text{h}$) is larger than that of cross section 2 ($16 \text{ kg s}^{-1}/2\text{h}$) (Fig. 6c). The value of horizontal velocity (u) increases above 5 m s^{-1} on the cross section 2 and pollutant concentration began to decreases at 2100 (Fig. 6c). Until 2200, the vertical velocity (w) changed into the upward (Fig. 6a), the increase rate of $\text{PM}_{2.5}$ flux decreases further (Fig. 6c and d), and pollutant concentration decreases. But it is worth noting that the PBLH is till decreasing, and thus the lower PBLH is an insufficient condition for the higher pollutant concentration. In short, not only the relative changes of pollutants in the horizontal direction should be paid attention to, but also the effect of vertical direction cannot be neglected. When the net pollutant flux is smaller in the horizontal direction, the vertical movement determines the change of pollutant concentration.

In order to better understand the role of advection transport and turbulent diffusion within the PBL during the CS, we quantitatively calculated the proportion of advection based on the mass conservation equation of pollutants (mainly consider advection, turbulence and source (sink) term)

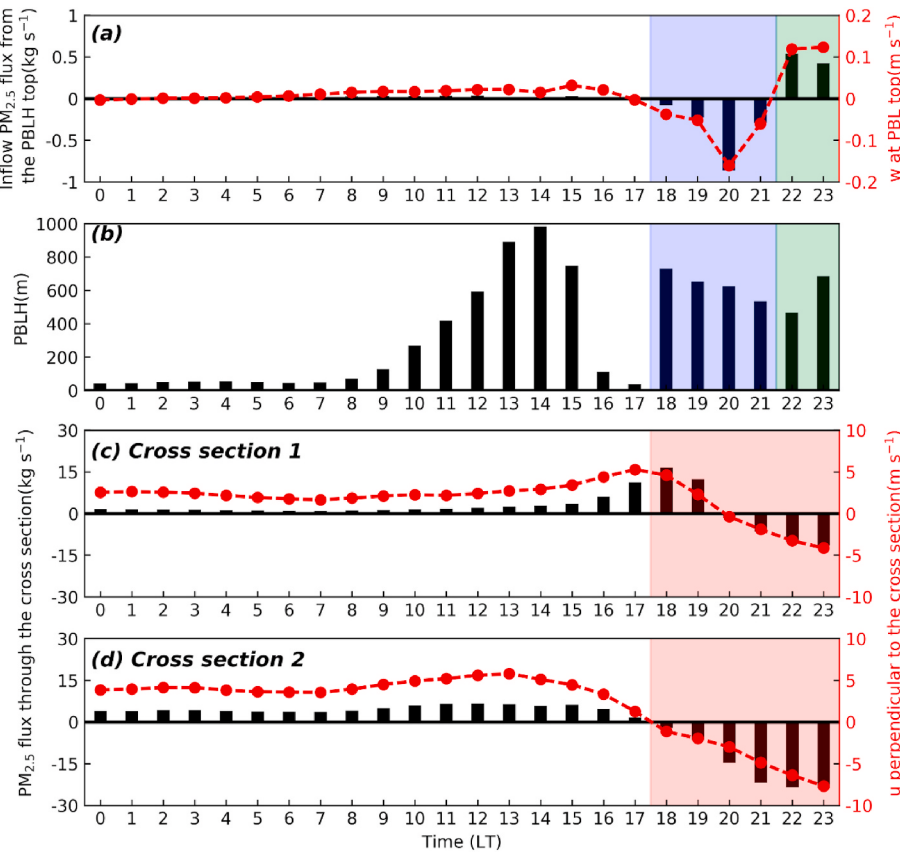


Fig. 6. Time series of (a) inflow of the PM_{2.5} flux (black bars) from the PBLH top and the vertical velocity (red dots-lines) at the PBL top level, (b) the PBLH in Anqing, (c-d) PM_{2.5} flux through the cross sections 1 and 2 on December 5, 2016. The average u-component of the horizontal wind (red dots-lines) perpendicular to the cross section. The purple shaded areas indicate the approximate periods when the pollutants transported from the residual layer to the PBL, and the green shaded areas indicate the pollutants within PBL transported to the residual layer. The red shaded areas indicate the approximate periods of significant change for the pollutant concentration. The locations of the cross section are marked by the red lines 1 and 2 in Fig. 1c. (For interpretation of the references to color in this figure legend, the reader is referred to the Web version of this article.)

$$\frac{\partial c}{\partial t} = -\bar{U}_i \frac{\partial \bar{c}}{\partial x_j} + \gamma_c \frac{\partial^2 \bar{c}}{\partial x_j^2} - \frac{\partial (\bar{U}_i' c')}{\partial x_j} + \bar{s}_{i..} \quad (1)$$

I II III IV V

where term I represents local storage term, term II describes the advection of pollutants by the mean wind, term III is the viscous dissipation of molecular, term IV represents the turbulent diffusion term, and term V is a term of source and sink. we can calculate the local storage term (i.e., pollutant concentration changing with time; term I) and the advection of pollutants by the mean wind (term II) from the simulation results. The U_i and x_j are expressed u , v , w and x , y , z , respectively. We use Anqing sounding station (30.37°N , 116.58°E) as the target grid point for calculation. The viscous dissipation of molecular term is ignored, and the source and sink term remain unchanged in a short period. Only advection transport and turbulent diffusion remain on the right side of Eq. (1). For the CS of three HPEs, the advection transport accounts for 7.8%~146% of the total pollutant concentration changes within the PBL. This result suggests that the turbulent diffusion term and the advection transport term have a synergistic effect on the change of pollutants. Therefore, the role of turbulent diffusion and advection transport are extremely important during the pollutant evolution process. In the future, the quantitative calculation of the pollutant concentration changes caused by the turbulent diffusion term need further study.

3.5. Variations of turbulence characteristics-microscale

The importance of turbulence in the pollution events has been mentioned above, so this section will discuss the change of turbulence characteristics from the dynamic, thermal and turbulent mixing. Turbulence is mainly divided into thermal turbulence and mechanical turbulence. Turbulent transport is one of the most important processes

within the PBL, and turbulence mixing determines the exchange of pollutants in the model. Therefore, this study selects three turbulence statistical parameters (i.e., represent the dynamic, thermal and mixing) to analyze the change of turbulence characteristics in the four HPEs. Firstly, the friction velocity u^* (units: m s^{-1}) is used to represent the dynamic characteristic of turbulence, which is calculated by Eq S(2). Secondly, the local Obukhov length is used to indicate atmospheric stratification stability, which is defined as Eq S(3). And the last parameter is turbulent diffusion coefficient (TDC), which is a vital parameter for the calculation of the pollutants during the boundary layer mixing process in the model. This parameter is parameterized by two methods in the ACM2 PBL parameterization scheme. The first method is calculated by friction velocity (u^*), nondimensional profile functions (ϕ) and PBLH (h) (Fig. S8a). Equation is as follows

$$K_z = \kappa \frac{u^*}{\phi} z (1 - z/h)^2 \quad (2)$$

where z is the height above ground, h is the PBLH (i.e., PBLH is defined as the height when the Richardson number (R_i) is equal to 0.25), κ is von Karman constant. ϕ is the nondimensional profile functions of heat (ϕ_h) and momentum (ϕ_m) (detail formula refers to Dyer, 1974). K_z represents the turbulent diffusion coefficients of heat (K_h), momentum (K_m) and water vapor (K_q). Note that when ϕ in Eq. (2) is replaced by ϕ_h , then K_z becomes K_h . The second method is calculated by wind shear (ss), Richardson number (R_i) and nondimensional functions (φ) (Fig. S8b). Equation is as follows

$$K_z = 0.01 + \sqrt{ss} \cdot \varphi \cdot \left(0.4z \frac{80}{80 + 0.4z} \right)^2, R_i \geq 0 \quad (3)$$

$$K_z = 0.01 + \sqrt{ss(1 - 25R_i)} \cdot \left(0.4z \frac{80}{80 + 0.4z} \right)^2, R_i < 0 \quad (4)$$

where ss is the wind shear, φ is a nondimensional function related to R_i . Then K_z takes the maximum of the two methods. In the ACM2 PBL parameterization scheme, the final $K(z)$ will be affected by K_z and a key parameter f_{conv} (i.e., $K(z) = K_z(1 - f_{conv})$). The expression of f_{conv} is denoted by the ratio of the nonlocal flux term to the total flux as Eq S(4).

It can be seen from Table S2, the PM_{2.5} concentration and friction velocity show a significant negative correlation ($R = -0.407 \sim -0.755$). Shi et al. (2019) also demonstrated the negative correlation between friction velocity and PM_{2.5} concentration by using the observational data of 325-m meteorological tower in Beijing. In addition, Wang et al. (2019) used the observational turbulence data of three levels during the same period (i.e., from December 1, 2016 to January 10, 2017) to prove that PM_{2.5} concentrations at the ground was significantly negative correlation with friction velocity and turbulent kinetic energy. Anqing is in the "mountain corridor", and wind speed is larger than other two cities. Even if the underlying surface of three cities is different, the wind speed and friction velocity are approximately linear (not shown). Therefore, the friction velocity is greater at longer transport stages in Anqing, the value of negative correlation is lower. The greater wind speed results in the stronger turbulent mixing, and the atmospheric stratification is closer to neutral stratification (the value of the reciprocal of Obukhov length (1/L) approaches 0). Similarly, the PM_{2.5} concentration and 1/L display a positive correlation ($R = 0.308 \sim 0.569$) (Table S2). It is worth stressing that the neutral stratification is conducive to the diffusion of local pollutants and transport pollutants from other regions to the local. Thus, the longer transport stages lead to the smaller correlation between PM_{2.5} concentration and 1/L in Anqing (Table S2). It is known that turbulent mixing plays a vital role in dissipating and transporting of pollutants, and the change of heat, momentum, vapor and pollutant fluxes depend on the TDC (Jia and Zhang, 2020; Shin and Hong, 2011). Table S2 shows the obvious negative correlation between PM_{2.5} concentration and TDC ($R = -0.392 \sim -0.724$). A smaller correlation coefficient between PM_{2.5} concentration and TDC in Anqing, because the TDC is changeable during several cleaning periods (i.e., the TDC from a

smaller value to a larger value in short time) (not shown). According to the calculation principle of TDC (Eqs. (2)–(4)), the saltation of the TDC may be caused by the change of wind shear in Anqing (Fig. S9). Due to the terrain, the wind shear in Anqing is significantly different from that in Fuyang, especially under the larger wind speed condition. To sum up, the higher PM_{2.5} concentration corresponds to smaller friction velocity, smaller TDC and strong stable stratifications. However, the turbulence characteristics at different stages (i.e., TS and CS) need further detailed analysis and demonstration.

For the HPE1-3 processes, with the gradually increasing PM_{2.5} concentration, the friction velocity showed a downward trend (Fig. 7a–c). During the HPE4 process in Anqing, the friction velocity not decreases significantly and has a synchronous increases trend with PM_{2.5} concentration (Fig. 7d). While the TDC decreases for each HPE, and not shows any obvious difference between these cities (Fig. 7i–l). From the beginning of the pollution event, as the PM_{2.5} concentration increases, the TDC of the HPE1–4 decreases by 48%, 74%, 89% and 69%, respectively. Among four HPEs, the PM_{2.5} concentration is the highest in HPE2 and HPE3, and the larger reduction ratio of TDC in these two HPEs.

As mentioned before, the TS lasted a longer time in Anqing than that of Fuyang during HPE4 (Figs. 2 and S3). In order to ensure the uniformity of the number of samples in the TS and CS, we only selected HPE1–3 to analyze the daily variation of the turbulence statistical parameters. Fig. 8 shows the daily variation of friction velocity, 1/L and TDC. No matter what underlying surface, the friction velocity in the TS is greater than that in the CS (Fig. 8a, d, g). Regardless of what stage of HPEs, the friction velocity in the Anqing is greater than that in the Fuyang (Fig. 8a, g). For the TS, the friction velocity is larger in the wee hours, mainly because it is gradually decreasing from the cleaning stages (Fig. 8a, d, g). Until the midnight, the friction velocity decreases to the same magnitude as the CS (0.1 m s^{-1}). The value of 1/L is closer to 0, and the near-surface atmosphere presents near-neutral stratification in the TS (Fig. 8b, e, h). For the CS, the atmosphere presents the strong stable stratification at nighttime, which is beneficial to the accumulation of

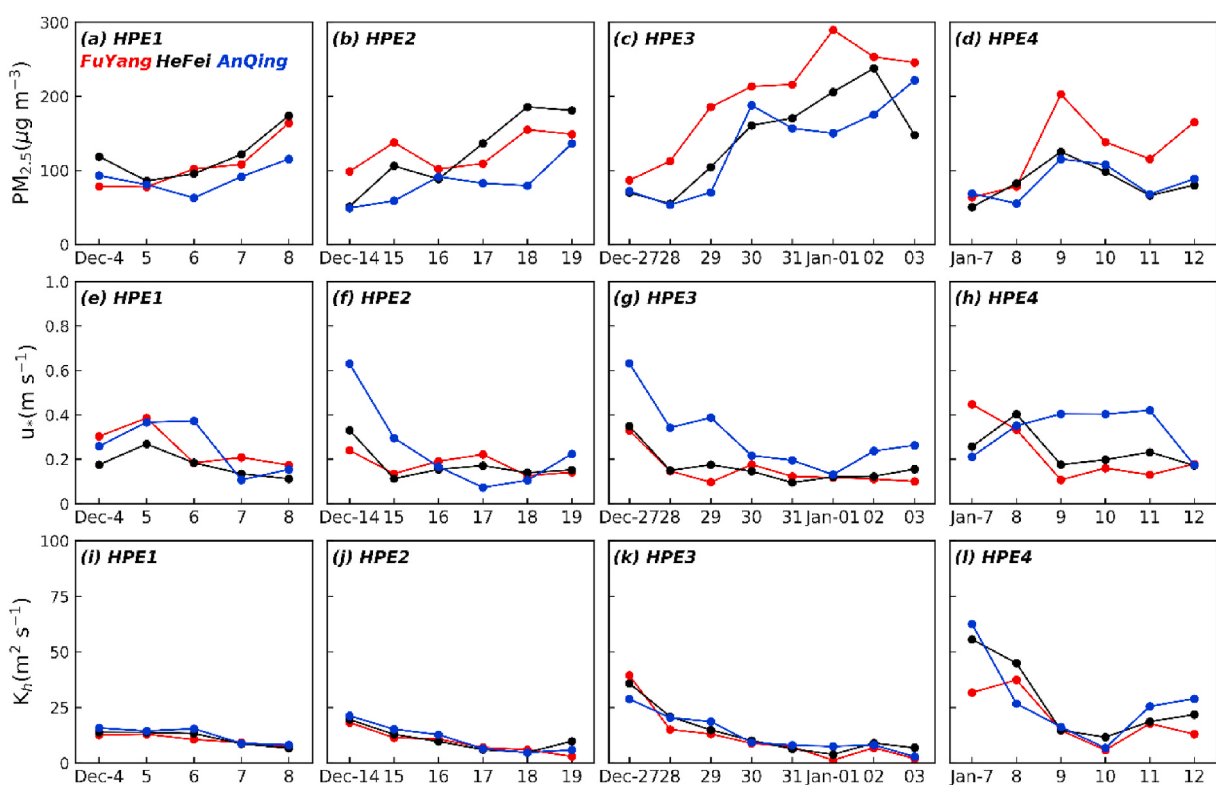


Fig. 7. Time series of (a–d) daily mean PM_{2.5} concentration, (e–h) friction velocity, and (i–l) turbulent diffusion coefficient from the simulation results in the HPE1–4 in Fuyang, Hefei and Anqing.

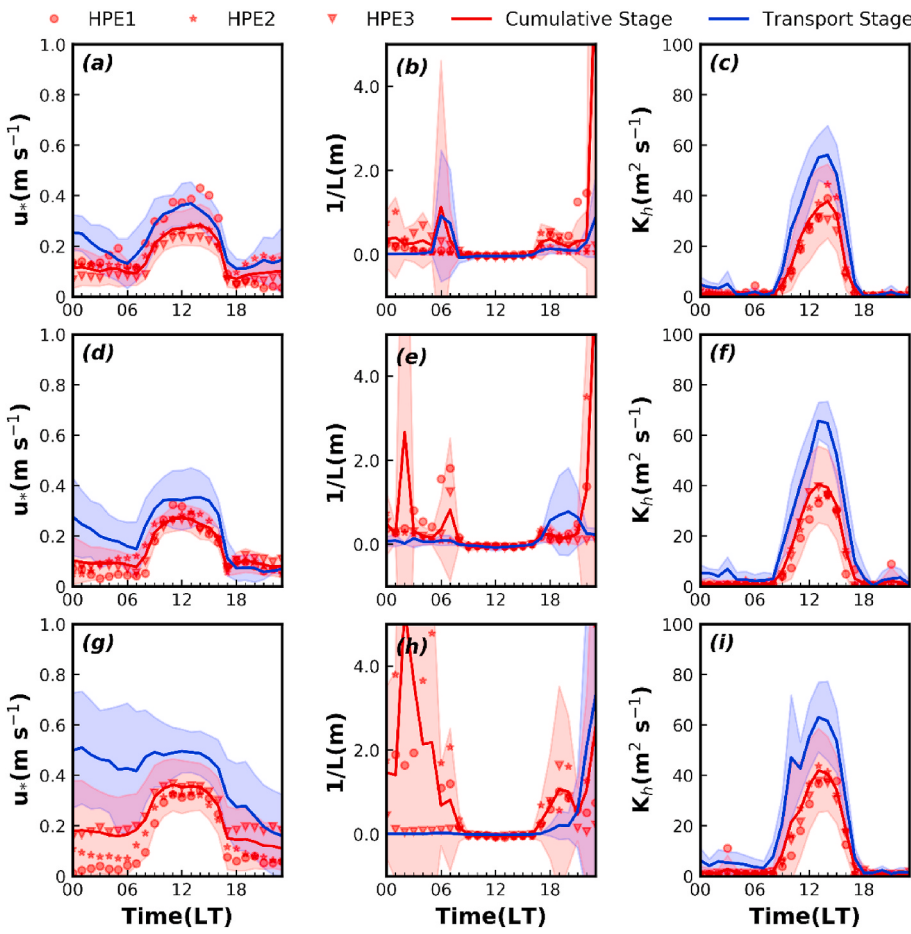


Fig. 8. Diurnal variations of friction velocity, reciprocal of the Obukhov length ($1/L$) and turbulent diffusion coefficient from the simulation results in (a–c) Fuyang, (d–f) Hefei and (g–i) Anqing. The blue lines denote the average value of transport stage, and the red lines represent the average value of cumulative stage during three HPEs. Different symbols denote different HPE and the shaded represents the mean value \pm standard deviation. (For interpretation of the references to color in this figure legend, the reader is referred to the Web version of this article.)

aerosol pollutants. Under the strong stable conditions, the turbulence is intermittent (Ren et al., 2019; Wang et al., 2018), and the model has insufficient performance for turbulence, which leads to large differences in the simulation of pollutant concentration. The knowledge of the

physical mechanism behind the intermittent behavior of turbulence in the stable boundary layer is still very limited, thus more observational data are needed to analyzed and better applied the model. The TDC of TS is larger than that of CS, and the difference of two stages is about 20 m^2

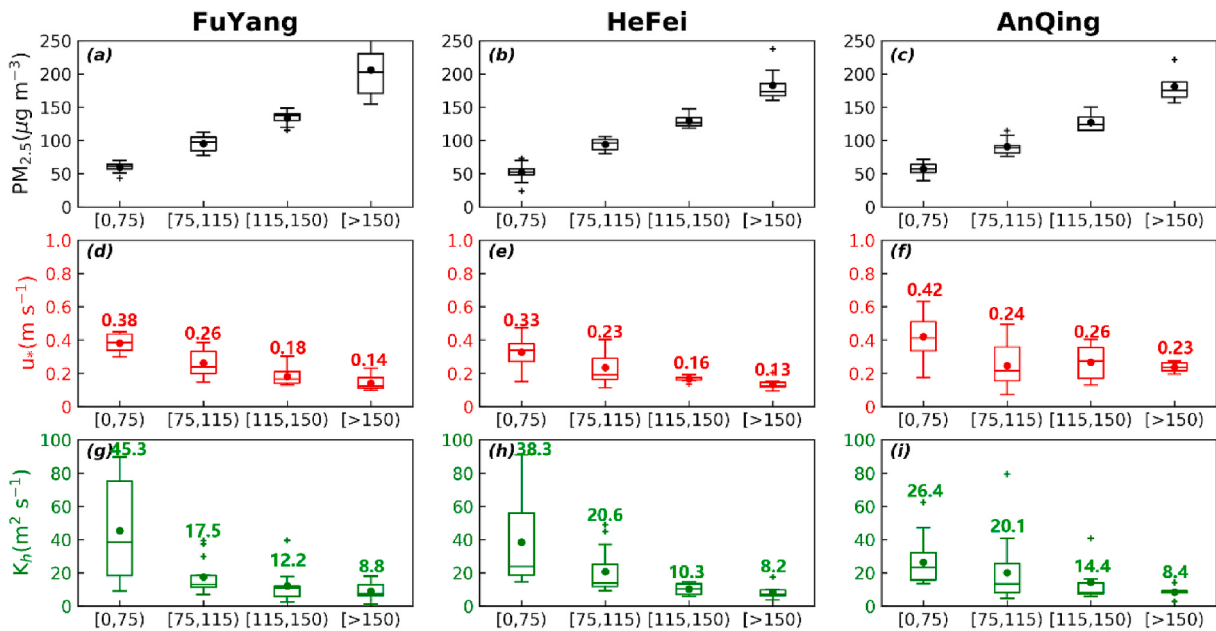


Fig. 9. Distribution of PM_{2.5} concentration in different ranges of friction velocity and turbulent diffusion coefficient from the simulation results in (a, d, g) Fuyang, (b, e, h) Hefei and (c, f, i) Anqing from December 2, 2016 to January 15, 2017.

s^{-1} ($4 \text{ m}^2 \text{ s}^{-1}$) during the daytime (nighttime) (Fig. 8c, f, i). In short, as the $\text{PM}_{2.5}$ concentration increases from below $75 \mu\text{g m}^{-3}$ to above $150 \mu\text{g m}^{-3}$, the friction velocity decreases 63%, 61% and 45%, respectively (Fig. 9a–c). And the TDC decreases 80%, 78% and 68%, respectively (Fig. 9d–f). In addition, it is worth noting that when the $\text{PM}_{2.5}$ concentration increases above $115 \mu\text{g m}^{-3}$, the friction velocity only decreases 7%–11%, and TDC only decreases 7%–23%. This result indicates that when the pollution level reaches above medium degree, as the pollutant concentration increases again, the degree of turbulence changes is decreases. That is, the change of pollutant is less sensitive to the change of turbulence during the HPEs.

3.6. Contributions of emission sources

Previous studies have reported that local emissions are the primary reason of heavy pollution episodes in China (Sun et al., 2014; Wu et al., 2017). Emission control measures can ensure good air quality for major events, such as Zhang et al. (2009) for the Olympic Monitoring Campaign, Tang et al. (2015) for the Asia-Pacific Economic Cooperation and Huang et al. (2020a) for the COVID-19. Up to now, many scholars have certified the contribution of regional transport and local emissions in the NCP (Wang et al., 2017), YRD (Liu et al., 2019), Two Lakes Basin (TLB) (Lu et al., 2019). However, there are some gaps for the contributions of the local emissions and regional transport in the YH region (i.e., located between YRD and LHP, and which is rarely followed by scholars), especially during the HPEs.

Fig. S10 quantitatively presents the contributions of local emissions, regional transport, synergistic interaction, and background field. From the time scale, Fuyang has the largest contribution of local emissions (51%), Hefei has the largest contribution of regional transport (45.3%), and Anqing has the largest contribution of synergistic interaction (13.3%). The contribution of the trans-boundary transport is about 48% (55.05%, 53.1%) in Fuyang (Hefei and Anqing), indicate that neighboring provinces contribute more pollutants. The difference between contributions of local emissions and regional transport is only 3%–11% in the YH region, which indicate that the contributions of these two aspects are equivalent in the YH region. During the TS, the contribution of regional transport can reach 68%. And contribution of local emissions is also as high as 61% during the CS in Fuyang (Fig. 10). The results of

Anqing and Hefei are similar to that of Fuyang. The contribution of regional transport is greater than that of local emissions in the TS. Similarly, the contribution of local emissions is the largest in the CS. In summary, the contributions of regional transport, local emissions and synergistic interaction reach 43%, 47% and 9%, respectively. We need pay attention to the contribution of each part during the HPEs, which will help us to build a certain foundation for the emission reduction work in the future.

4. Conclusions

To elucidate the pollutant evolution mechanism during the heavy pollution episodes (HPEs) in the Yangtze-Huaihe (YH) valley in winter 2016, this study combined observational data analysis and three-dimensional meteorology-chemistry coupled simulations from a multi-scale perspective. On the basis of the wintertime $\text{PM}_{2.5}$ measurements and radiosonde data in Fuyang and Anqing from 2 December 2016 to January 15, 2017, the relationships between PBL structure and aerosol pollution were examined. Meanwhile, four HPEs and two stages (i.e., transport stage, TS and cumulative stage, CS) of each HPE are defined. Results show the following.

- From a macroscale perspective: There are four HPEs in Yangtze-Huaihe (YH) region, but three HPEs in Beijing-Tianjin-Hebei (BTH) region. The $\text{PM}_{2.5}$ concentration dropped sharply in the BTH region, which began to rise during the HPE1 in the YH region. For the HPE2 and HPE3, the $\text{PM}_{2.5}$ concentration increases almost simultaneously in the YH and BTH regions, and decreases earlier in the YH region. The $\text{PM}_{2.5}$ concentration began to increases during the HPE4 in the YH region, and the BTH region is undergoing the dissipative stage of HPE3. The pollution situation of the YH region was controlled by synoptic systems (Fig. 11a).
- From a mesoscale perspective: During the long-distance transportation of pollutants from the BTH to the YH region, the pollutants are first transported to the northern of YH through the near-surface layer. Then, the pollutants will be transported to the “mountain corridor” region with wind direction changes. It is worth nothing that there is an important residual layer (i.e., RL) transport mechanism during the TS in the “mountain corridor”. During the process of

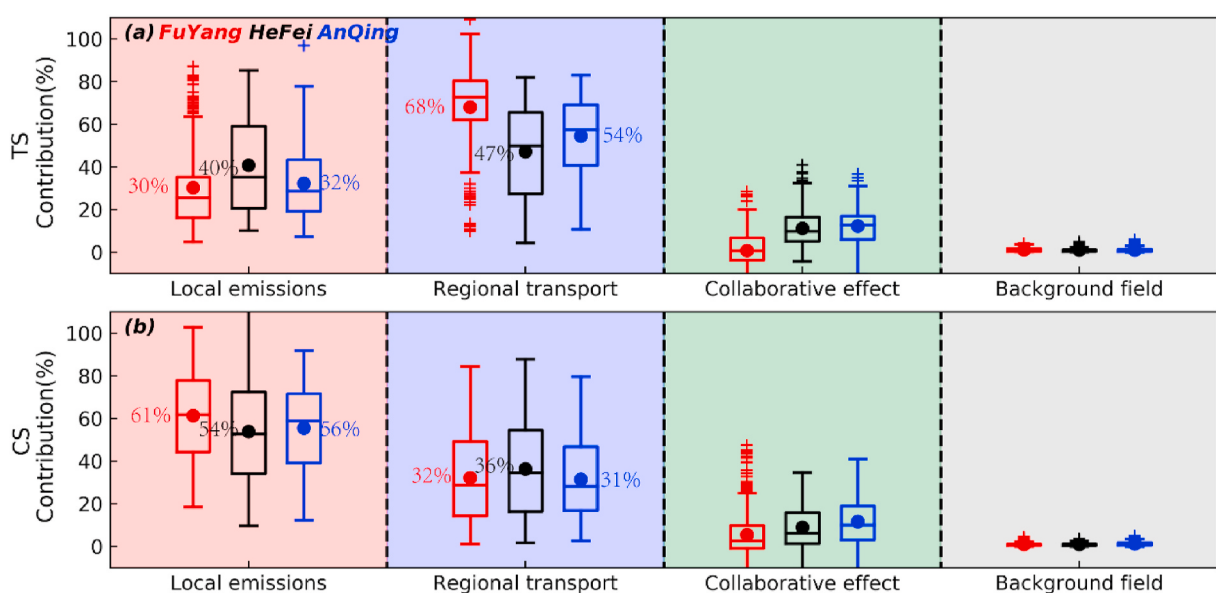


Fig. 10. Box-Whiskers plots owing the contributions of local emissions, regional transport, collaborative effect and background field from the simulation results in the (a) TS and (b) CS during 4 HPEs in Fuyang, Hefei and Anqing. Different background colors represent different contributions, pink, light blue, green and gray represent the contributions of local emissions, regional transport, collaborative effect and background field, respectively. (For interpretation of the references to color in this figure legend, the reader is referred to the Web version of this article.)

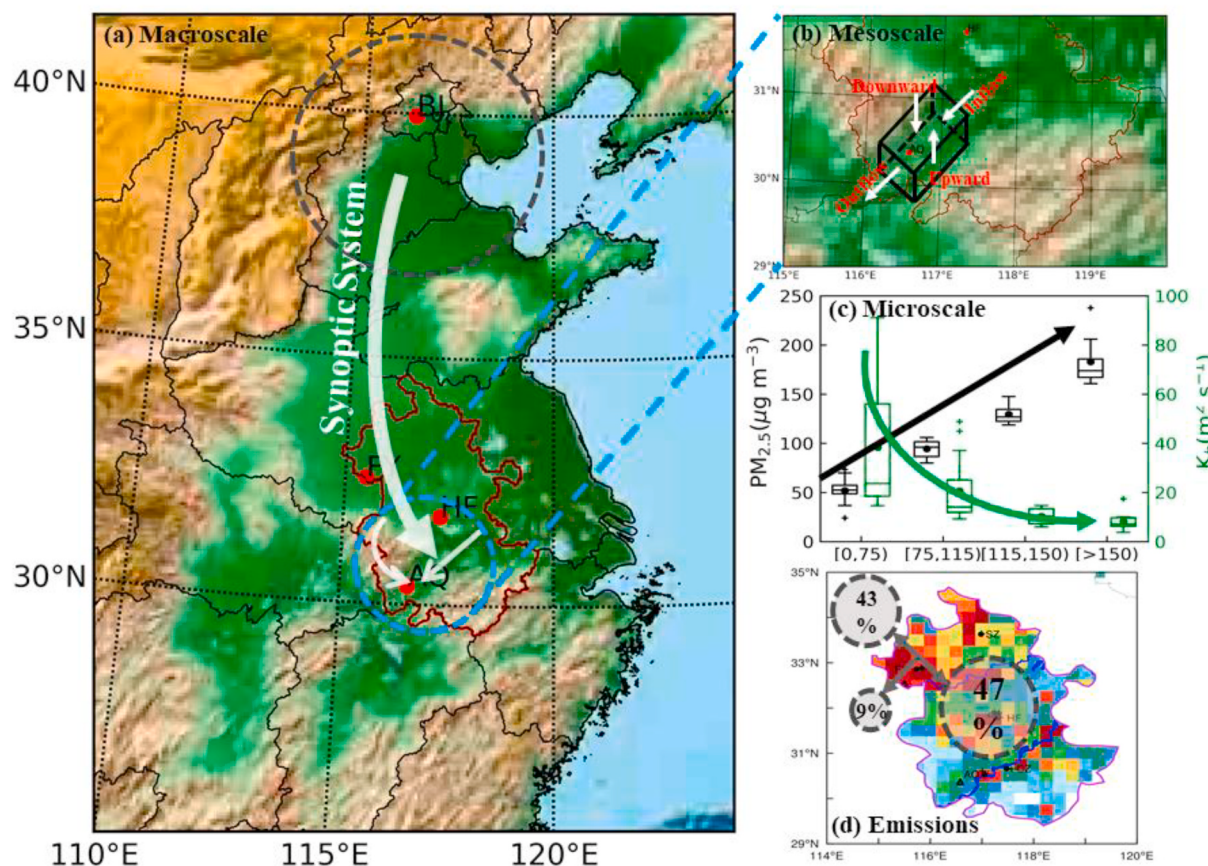


Fig. 11. Diagrammatic sketch of the pollutant evolution mechanism by multiscale processes (a) macroscale, (b) mesoscale, (c) microscale, and (d) contributions of emission sources.

the pollutant concentration changes, not only the relative changes of horizontal pollutants should be paid attention to, but also the effect of vertical direction cannot be ignored (Fig. 11b). For the CS of three HPEs, based on the mass conservation equation of pollutants, the advection transport accounts for 7.8%~146% of the total pollutant concentration changes within the PBL. This result indicates that the turbulent diffusion and the advection transport have a synergistic effect on the change of pollutant. In addition, quantitative analysis of turbulent diffusion and source and sink term are warranted further studies.

- From a microscale perspective: As the wind speed increases, the near-surface will change to the near-neutral stratification and friction velocity increases, which is conducive to the diffusion of local pollutants and transported pollutants from other regions to the local. The stronger wind shear in the “mountains corridor” will affect the change of turbulent diffusion coefficient (TDC) in the model. In addition, the turbulence characteristics are significantly different during the TS and CS, especially the strong stable conditions occurred in the CS at nighttime. In short, as the $\text{PM}_{2.5}$ concentration linear increases from below $75 \mu\text{g m}^{-3}$ to above $150 \mu\text{g m}^{-3}$, the friction velocity decreases 63%, 61% and 45%, respectively. And the TDC decreases 80%, 78% and 68%, respectively. Therefore, the change of pollutants is less sensitive to the change of turbulence during the HPEs (Fig. 11c). In the future, more observational data are needed to analyzed and better applied the model.

- Finally, the contributions of local emissions and regional transport were demonstrated through three sensitivity experiments and one basic experiment. The contribution of regional transport, local emissions and synergistic interaction can reach 43%, 47% and 9%, respectively (Fig. 11d). Thus we need pay attention to the

contribution of each part during the HPEs, which will help us to build a certain foundation for the emission reduction work in the future.

CRediT authorship contribution statement

Wenxing Jia: Conceptualization, Data curation, Formal analysis, Writing - original draft. **Xiaoye Zhang:** Conceptualization, Data curation, Writing - review & editing. **Yaqiang Wang:** Data curation, Writing - review & editing.

Declaration of competing interest

The authors declare that they have no known competing financial interests or personal relationships that could have appeared to influence the work reported in this paper.

Acknowledgements

This research is supported by the NSFC Project (U19A2044); National Key Project of MOST (2016YFC0203306); Atmospheric Pollution Control of the Prime Minister Fund (DQGG0104); Key Projects of Fundamental Scientific Research Fund of CAMS (2017Z001); Post-graduate Research & Practice Innovation Program of Jiangsu Province (KYCX20_0923). The authors would like to acknowledge the Tsinghua University for the support of emission data.

Appendix A. Supplementary data

Supplementary data to this article can be found online at <https://doi.org/10.1016/j.atmosenv.2020.117986>.

References

- Ackermann, I.J., Hass, H., Memmesheimer, M., Ebel, A., Binkowski, F.S., Shankar, U., 1998. Modal aerosol dynamics model for Europe. *Atmos. Environ.* 32, 2981–2999. [https://doi.org/10.1016/S1352-2310\(98\)00006-5](https://doi.org/10.1016/S1352-2310(98)00006-5).
- Bian, J., Chen, H., Holger, V., Duan, Y., Xuan, Y., Lv, D., 2011. Intercomparison of humidity and temperature sensors: GTS1, vaisala RS80, and CFH. *Adv. Atmos. Sci.* 28, 139–146. <https://doi.org/10.1007/s00376-010-9170-8>.
- Carnevale, C., Pisoni, E., Volta, M., 2010. A non-linear analysis to detect the origin of PM₁₀ concentrations in Northern Italy. *Sci. Total Environ.* 409, 182–191. <https://doi.org/10.1016/j.scitotenv.2010.09.038>.
- Chen, F., Dudhia, J., 2001. Coupling an advanced land surface–hydrology model with the Penn State–NCAR MM5 modeling system. Part I: model implementation and sensitivity. *Mon. Weather Rev.* 129, 569–585. [https://doi.org/10.1175/1520-0493\(2001\)129<0569:CAALSH>2.0.CO;2](https://doi.org/10.1175/1520-0493(2001)129<0569:CAALSH>2.0.CO;2).
- Deng, X., Shi, C., Wu, B., Chen, Z., Nie, S., He, D., Zhang, H., 2012. Analysis of aerosol characteristics and their relationships with meteorological parameters over Anhui province in China. *Atmos. Res.* 109–110, 52–63. <https://doi.org/10.1016/j.atmosres.2012.02.011>.
- Deng, X., Shi, C., Yao, C., Wu, B., Yang, Y., Zhang, H., 2015. Research of reconstruction and characteristics of hazes in Anhui. *Plateau Meteor.* 34, 1158–1166. <https://doi.org/10.7552/j.issn.1000-0534.2014.00007> (in Chinese).
- Ding, A., Huang, X., Nie, W., Sun, J., Kerminen, V., Petaja, T., Su, H., Cheng, Y., Yang, X., Wang, M., Chi, X., Wang, J., Virkkula, A., Guo, W., Yuan, J., Wang, S., Zhang, R., Wu, Y., Song, Y., Zhu, T., Zilitinkevich, S., Kulmala, M., Fu, C., 2016a. Enhanced haze pollution by black carbon in megacities in China. *Geophys. Res. Lett.* 43, 2873–2879. <https://doi.org/10.1002/2016GL067745>.
- Ding, A., Nie, W., Huang, X., Chi, X., Sun, J., Kerminen, V.M., Xu, Z., Guo, W., Petaja, T., Yang, X., Kulmala, M., Fu, C., 2016b. Long-term observation of air pollution–weather/climate interactions at the SORPES station: a review and outlook. *Front. Environ. Sci. Eng.* 10, 15. <https://doi.org/10.1007/s11783-016-0877-3>.
- Dyer, A.J., 1974. A review of flux-profile relationships. *Bound-Layer. Meteorol.* 7, 363–372. <https://doi.org/10.1007/BF00240838>.
- Gabus, V., Pisoni, E., Volta, M., 2008. Factor separation in air quality simulations. *Ecol. Model.* 218, 383–392. <https://doi.org/10.1016/j.ecolmodel.2008.07.030>.
- Grell, G.A., Devenyi, D., 2002. A generalized approach to parameterizing convection combining ensemble and data assimilation techniques. *Geophys. Res. Lett.* 29, 1693. <https://doi.org/10.1029/2002GL015311>.
- Grell, G.A., Peckham, S.E., Schmitz, R., McKeen, S.A., Frost, G., Skamarock, W.C., Eder, B., 2005. Fully coupled “online” chemistry within the WRF model. *Atmos. Environ.* 39, 6957–6975. <https://doi.org/10.1016/j.atmosenv.2005.04.027>.
- Guo, J., Miao, Y., Zhang, Y., Liu, H., Li, Z., Zhang, W., He, J., Lou, M., Yan, Y., Bian, L., Zhai, P., 2016. The climatology of planetary boundary layer height in China derived from radiosonde and reanalysis data. *Atmos. Chem. Phys.* 16, 13309–13319. <https://doi.org/10.5194/acp-16-13309-2016>.
- Huang, S., Liu, F., Sheng, L., Cheng, L., Wu, L., Li, J., 2018. On adjoint method based atmospheric emission source tracing. *Chin. Sci. Bull.* 63, 1594–1605. <https://doi.org/10.1360/N972018-00196> (in Chinese).
- Huang, X., Ding, A., Gao, J., Zheng, B., Zhou, D., Qi, X., Tang, R., Ren, C., Nie, W., Chi, X., Wang, J., Xu, Z., Chen, L., Li, Y., Che, F., Pang, N., Wang, H., Tong, D., Qin, W., Cheng, W., Liu, W., Fu, Q., Chai, F., Davis, S.J., Zhang, Q., He, K., 2020a. Enhanced secondary pollution offset reduction of primary emissions during COVID-19 lockdown in China. *Natl. Sci. Rev. nwaal37* <https://doi.org/10.1093/nsr/nwaal37>.
- Huang, X., Ding, A., Wang, Z., Ding, K., Gao, J., Chai, F., Fu, C., 2020b. Amplified transboundary transport of haze by aerosol-boundary layer interaction in China. *Nat. Geosci.* 13, 428–434. <https://doi.org/10.1038/s41561-020-0583-4>.
- Iacono, M.J., Delamere, J.S., Mlawer, E.J., Shephard, M.W., Clough, S.A., Collins, W.D., 2008. Radiative forcing by long-lived greenhouse gases: calculations with the AER radiative transfer models. *J. Geophys. Res. Atmos.* 113, D13103. <https://doi.org/10.1029/2008JD009944>.
- Jia, W., Zhang, X., 2020. The role of the planetary boundary layer parameterization schemes on the meteorological and aerosol pollution simulations: a review. *Atmos. Res.* 239, 104890. <https://doi.org/10.1016/j.atmosres.2020.104890>.
- Jimenez, P.A., Dudhia, J., 2012. Improving the representation of resolved and unresolved topographic effects on surface wind in the WRF model. *J. Appl. Meteorol. Climatol.* 51, 300–316. <https://doi.org/10.1175/JAMC-D-11-084.1>.
- Kusaka, H., Kondo, H., Kikegawa, Y., Kimura, F., 2001. A simple single-layer urban canopy model for atmospheric models: comparison with multi-layer and slab models. *Bound-Layer. Meteorol.* 101, 329–358. <https://doi.org/10.1023/a:1019207923078>.
- Li, X., Wang, Y., Shen, L., Zhang, H., Zhao, H., Zhang, Y., Ma, Y., 2018. Characteristics of boundary layer structure during a persistent haze event in the central Liaoning city cluster, northeast China. *J. Meteorol. Res.* 32, 302–312. <https://doi.org/10.1007/s13351-018-7053-6>.
- Li, Z., Guo, J., Ding, A., Liao, H., Liu, J., Sun, Y., Wang, T., Xue, H., Zhang, H., Zhu, B., 2017. Aerosol and boundary-layer interactions and impact on air quality. *Natl. Sci. Rev.* 4, 810–833. <https://doi.org/10.1093/nsr/nwx117>.
- Liao, T., Gui, K., Jiang, W., Wang, S., Wang, B., Zeng, Z., Che, H., Wang, Y., Sun, Y., 2018. Air stagnation and its impact on air quality during winter in Sichuan and Chongqing, southwestern China. *Sci. Total Environ.* 635, 576–585. <https://doi.org/10.1016/j.scitotenv.2018.04.122>.
- Lin, Y.L., Farley, R.D., Orville, H.D., 1983. Bulk parameterization of the snow field in a cloud model. *J. Clim. Appl. Meteorol.* 22, 1065–1092. [https://doi.org/10.1175/1520-0450\(1983\)022<1065:BPOTSF>2.0.CO;2](https://doi.org/10.1175/1520-0450(1983)022<1065:BPOTSF>2.0.CO;2).
- Liu, J., Shen, J., Cheng, Z., Wang, P., Ying, Q., Zhao, Q., Zhang, Y., Zhao, Y., Fu, Q., 2019. Source apportionment and regional transport of anthropogenic secondary organic aerosol during winter pollution periods in the Yangtze River Delta, China. *Sci. Total Environ.* 710, 135620. <https://doi.org/10.1016/j.scitotenv.2019.135620>.
- Liu, L., Guo, J., Miao, Y., Liu, L., Li, J., Chen, D., He, J., Cui, C., 2018. Elucidating the relationship between aerosol concentration and summertime boundary layer structure in central China. *Environ. Pollut.* 241, 646–653. <https://doi.org/10.1016/j.envpol.2018.06.008>.
- Lo, J.C., Lau, A.K., Fung, J.C., Chen, F., 2006. Investigation of enhanced cross-city transport and trapping of air pollutants by coastal and urban land-sea breeze circulations. *J. Geophys. Res. Atmos.* 111, D14104. <https://doi.org/10.1029/2005JD006837>.
- Lu, M., Tang, X., Wang, Z., Wu, L., Chen, X., Liang, S., Zhou, H., Wu, H., Hu, K., Shen, L., Yu, J., Zhu, J., 2019. Investigating the transport mechanism of PM_{2.5} pollution during January 2014 in Wuhan, Central China. *Adv. Atmos. Sci.* 36, 1217–1234. <https://doi.org/10.1007/s00376-019-8260-5>.
- Ma, Y., Ye, J., Xin, J., Zhang, W., Arellano, J.V.G., Wang, S., Zhao, D., Dai, L., Ma, Y., Wu, X., Xia, X., Tang, G., Wang, Y., Shen, P., Lei, Y., Martin, S.T., 2020. The stove, dome, and umbrella effects of atmospheric aerosol on the development of the planetary boundary layer in haze regions. *Geophys. Res. Lett.* 47 <https://doi.org/10.1029/2020GL087373>.
- Miao, Y., Guo, J., Liu, S., Zhao, C., Li, X., Zhang, G., Wei, W., Ma, Y., 2018a. Impacts of synoptic condition and planetary boundary layer structure on the trans-boundary aerosol transport from Beijing-Tianjin-Hebei region to northeast China. *Atmos. Environ.* 181, 1–11. <https://doi.org/10.1016/j.atmosenv.2018.03.005>.
- Miao, Y., Liu, S., Guo, J., Huang, S., Yan, Y., Lou, M., 2018b. Unraveling the relationships between boundary layer height and PM_{2.5} pollution in China based on four-year radiosonde measurements. *Environ. Pollut.* 243, 1181–1195. <https://doi.org/10.1016/j.envpol.2018.09.070>.
- Miao, Y., Liu, S., Huang, S., 2019. Synoptic pattern and planetary boundary layer structure associated with aerosol pollution during winter in Beijing, China. *Sci. Total Environ.* 682, 464–474. <https://doi.org/10.1016/j.scitotenv.2019.05.199>.
- Ning, G., Wang, S., Yim, S.H.L., Li, J., Hu, Y., Shang, Z., Wang, J., Wang, K., 2018. Impact of low-pressure systems on winter heavy air pollution in the northwest Sichuan Basin, China. *Atmos. Chem. Phys.* 18, 13601–13615. <https://doi.org/10.5194/acp-18-13601-2018>.
- Ning, G., Yim, S.H.L., Wang, S., Duan, B., Nie, C., Yang, X., Wang, J., Shang, K., 2019. Synergistic effects of synoptic weather patterns and topography on air quality: a case of the Sichuan Basin of China. *Clim. Dynam.* <https://doi.org/10.1007/s00382-019-04954-3>.
- Plein, J.E., 2007. A combined local and nonlocal closure model for the atmospheric boundary layer. Part I: model description and testing. *J. Appl. Meteorol. Climatol.* 46, 1383–1395. <https://doi.org/10.1175/JAM2539.1>.
- Ren, Y., Zhang, H., Wei, W., Wu, B., Cai, X., Song, Y., 2019. Effects of turbulence structure and urbanization on the heavy haze pollution process. *Atmos. Chem. Phys.* 19, 1041–1057. <https://doi.org/10.5194/acp-19-1041-2019>.
- Schell, B., Ackermann, I.J., Hass, H., 2001. Modeling the formation of secondary organic aerosol within a comprehensive air quality model system. *J. Geophys. Res.* 106, 28275–28293. <https://doi.org/10.1029/2001JD000384>.
- Seidel, D.J., Ao, C.O., Li, K., 2010. Estimating climatological planetary boundary layer heights from radiosonde observations: comparison of methods and uncertainty analysis. *J. Geophys. Res. Atmos.* 115, D16113. <https://doi.org/10.1029/2009JD013680>.
- Seidel, D.J., Zhang, Y., Beljaars, A., Golaz, J.C., Jacobson, A.R., Medeiros, B., 2012. Climatology of the planetary boundary layer over the continental United States and Europe. *J. Geophys. Res. Atmos.* 117, D17106. <https://doi.org/10.1029/2012JD018143>.
- Shi, C., Yuan, R., Wu, B., Meng, Y., Zhang, H., Zhang, H., Gaong, Z., 2018a. Meteorological conditions conducive to PM_{2.5} pollution in winter 2016/2017 in the western Yangtze River Delta, China. *Sci. Total Environ.* 642, 1221–1232. <https://doi.org/10.1016/j.scitotenv.2018.06.137>.
- Shi, C., Zhang, H., Yang, Y., Zhang, H., 2018b. The trend of persistent regional haze in Anhui Province and corresponding characteristics of aerosol pollution. *China Environ. Sci.* 38, 1231–1242. <https://doi.org/10.3969/j.issn.1000-6923.2018.04.003> (in Chinese).
- Shi, Y., Hu, F., Lv, R., He, Y., 2019. Characteristics of urban boundary layer in heavy haze process based on Beijing 325m tower data. *Atmos. Oceanogr. Sci. Libr.* 12, 41–49. <https://doi.org/10.1080/16742834.2019.1547084>.
- Shin, H.H., Hong, S.Y., 2011. Intercomparison of planetary boundary-layer parametrizations in the WRF model for a single day from CASES-99. *Bound-Layer. Meteorol.* 139, 261–281. <https://doi.org/10.1007/s10546-010-9583-z>.
- Streets, D.G., Fu, J.S., Jang, C.J., Hao, J., He, K., Tang, X., Zhang, Y., Wang, Z., Li, Z., Zhang, Q., Wang, L., Wang, B., Yu, C., 2007. Air quality during the 2008 Beijing Olympic games. *Atmos. Environ.* 41, 480–492. <https://doi.org/10.1016/j.jatmosenv.2006.08.046>.
- Stull, R.B., 1988. An Introduction to Boundary Layer Meteorology. Springer Netherlands, Dordrecht. <https://doi.org/10.1007/978-94-009-3027-8>.
- Sun, Y., Jiang, Q., Wang, Z., Fu, P., Li, J., Yang, T., Yin, Y., 2014. Investigation of the sources and evolution processes of severe haze pollution in Beijing in January 2013. *J. Geophys. Res. Atmos.* 119, 4380–4398. <https://doi.org/10.1002/2014JD021641>.
- Tang, G., Zhu, X., Hu, B., Xin, J., Wang, L., Munkel, C., Mao, G., Wang, Y., 2015. Impact of emission controls on air quality in Beijing during APEC 2014: lidar ceilometer observations. *Atmos. Chem. Phys.* 15, 12667–12680. <https://doi.org/10.5194/acp-15-12667-2015>.

- Vogelezang, D.H.P., Holtslag, A.A.M., 1996. Evaluation and model impacts of alternative boundary-layer height formulations. *Bound-Layer. Meteorol.* 84, 245–269. <https://doi.org/10.1007/BF02430331>.
- Wang, H., Peng, Y., Zhang, X., Liu, H., Zhang, M., Che, H., Cheng, Y., Zheng, Y., 2018. Contributions to the explosive growth of PM_{2.5} mass due to aerosol-radiation feedback and decrease in turbulent diffusion during a red alert heavy haze in Beijing-Tianjin-Hebei, China. *Atmos. Chem. Phys.* 18, 17717–17733. <https://doi.org/10.5194/acp-18-17717-2018>.
- Wang, L., Wang, H., Liu, J., Gao, Z., Yang, Y., Zhang, X., Li, Y., Huang, M., 2019. Impacts of the near-surface urban boundary layer structure on PM_{2.5} concentrations in Beijing during winter. *Sci. Total Environ.* 669, 493–504. <https://doi.org/10.1016/j.scitotenv.2019.03.097>.
- Wang, Y., Bao, S., Wang, S., Hu, Y., Shi, X., Wang, J., Zhao, B., Jiang, J., Zheng, M., Wu, M., Russell, A.G., Wang, Y., Hao, J., 2017. Local and regional contributions to fine particulate matter in Beijing during heavy haze episodes. *Sci. Total Environ.* 580, 283–296. <https://doi.org/10.1016/j.scitotenv.2016.12.127>.
- Wang, Y., Ying, Q., Hu, J., Zhang, H., 2014a. Spatial and temporal variations of six criteria air pollutants in 31 provincial capital cities in China during 2013–2014. *Environ. Int.* 73, 413–422. <https://doi.org/10.1016/j.envint.2014.08.016>.
- Wang, Z., Liu, D., Wang, Z., Wang, Y., Khatri, P., Zhou, J., Takamura, T., Shi, G., 2014b. Seasonal characteristics of aerosols optical properties at the SKYNET Hefei site (31.90 °N, 117.17 °E) from 2007 to 2013. *J. Geophys. Res. Atmos.* 119, 6128–6139. <https://doi.org/10.1002/2014JD021500>.
- Wilcox, E.M., Thomas, R.M., Praveen, P.S., Pistone, K., Bender, F.A.M., Ramanathan, V., 2016. Black carbon solar absorption suppresses turbulence in the atmospheric boundary layer. *Proc. Natl. Acad. Sci. Unit.* 113, 11794–11799. <https://doi.org/10.1073/pnas.1525746113>.
- Wu, J., Li, G., Cao, J., Bei, N., Wang, Y., Feng, T., Huang, R., Liu, S., Zhang, Q., Tie, X., 2017. Contributions of trans-boundary transport to summertime air quality in Beijing, China. *Atmos. Chem. Phys.* 17, 2035–2051. <https://doi.org/10.5194/acp-17-2035-2017>.
- Wu, M., Wu, D., Fan, Q., Wang, B., Li, H., Fan, S., 2013. Observational studies of the meteorological characteristics associated with poor air quality over the Pearl River Delta in China. *Atmos. Chem. Phys.* 13, 10755–10766. <https://doi.org/10.5194/acp-13-10755-2013>.
- Yamada, T., 1976. On the similarity functions A, B and C of the planetary boundary layer. *J. Atmos. Sci.* 33, 781–793. [https://doi.org/10.1175/1520-0469\(1976\)0332.0.CO_2](https://doi.org/10.1175/1520-0469(1976)0332.0.CO_2).
- Yang, Y., Zheng, X., Gao, Z., Wang, H., Wang, T., Li, Y., Lau, G.N.C., Yim, S.H.L., 2018. Long-term trends of persistent synoptic circulation events in planetary boundary layer and their relationships with haze pollution in winter half year over eastern China. *J. Geophys. Res. Atmos.* 123, 1091–11007. <https://doi.org/10.1029/2018JD028982>.
- Ye, X., Song, Y., Cai, X., Zhang, H., 2016. Study on the synoptic flow patterns and boundary layer process of the severe haze events over the North China Plain in January 2013. *Atmos. Environ.* 124, 129–145. <https://doi.org/10.1016/j.scitotenv.2015.06.011>.
- Zhang, H., Zhang, X., Li, Q., Cai, X., Fan, S., Song, Y., Hu, F., Che, H., Quan, J., Kang, L., Zhu, T., 2020. Research progress on estimation of the atmospheric boundary layer height. *J. Meteor. Res.* 34, 4482–4498. <https://doi.org/10.1007/s13351-020-9910-3>.
- Zhang, L., Guo, X., Zhao, T., Gong, S., Xu, X., Li, Y., Luo, L., Gui, K., Wang, H., Zheng, Y., Yin, X., 2019. A modelling study of the terrain effects on haze pollution in the Sichuan Basin. *Atmos. Environ.* 196, 77–85. <https://doi.org/10.1016/j.atmosenv.2018.10.007>.
- Zhang, Q., Zheng, Y., Tong, D., Shao, M., Wang, S., Zhang, Y., Xu, X., Wang, J., He, H., Liu, W., Ding, Y., Lei, Y., Li, J., Wang, Z., Zhang, X., Wang, Y., Cheng, J., Liu, Y., Shi, Q., Yan, L., Geng, G., Hong, C., Li, M., Liu, F., Zheng, B., Cao, J., Ding, A., Gao, J., Fu, Q., Huo, J., Liu, B., Liu, Z., Yang, F., He, K., Hao, J., 2019. Drivers of improved PM_{2.5} air quality in China from 2013 to 2017. *Proc. Natl. Acad. Sci. Unit. States Am.* 116, 24463–24469. <https://doi.org/10.1073/pnas.1907956116>.
- Zhang, R., Wang, G., Guo, S., Zamora, M.L., Ying, Q., Lin, Y., Wang, W., Hu, M., Wang, Y., 2015. Formation of urban fine particulate matter. *Chem. Rev.* 115, 3803–3855. <https://doi.org/10.1021/cr5b00067>.
- Zhang, W., Guo, J., Miao, Y., Liu, H., Song, Y., Fang, Z., He, J., Lou, M., Yan, Y., Li, Y., Zhai, P., 2018. On the summertime planetary boundary layer with different thermodynamic stability in China: a radiosonde perspective. *J. Clim.* 31, 1451–1465. <https://doi.org/10.1175/JCLI-D-17-0231.s1>.
- Zhang, X., Wang, Y., Lin, W., Zhang, M., Zhang, X., Gong, S., Zhai, P., Yang, Y., Wang, J., Hou, Q., Zhang, X., Che, H., Guo, J., Li, Y., 2009. Changes of atmospheric composition and optical properties over Beijing 2008 olympic monitoring Campaign. *Bull. Am. Meteorol. Soc.* 90, 1633–1651. <https://doi.org/10.1175/2009BAMS2804.1>.
- Zhang, X., Xu, X., Ding, Y., Liu, Y., Zhang, H., Wang, Y., Zhong, J., 2019. The impact of meteorological changes from 2013 to 2017 on PM_{2.5} mass reduction in key regions in China. *Sci. China Earth Sci.* 62, 1–18. <https://doi.org/10.1007/s11430-019-9343-3>.
- Zhao, S., Yu, Y., Yin, D., He, J., Liu, N., Qu, J., Xiao, J., 2016. Annual and diurnal variations of gaseous and particulate pollutants in 31 provincial capital cities based on in situ air quality monitoring data from China National Environmental Monitoring Center. *Environ. Int.* 86, 92–106. <https://doi.org/10.1016/j.scitotenv.2015.11.003>.
- Zheng, Y., Che, H., Xia, X., Wang, Y., Wang, H., Wu, Y., Tao, J., Zhao, H., An, L., Li, L., Gui, K., Sun, T., Li, X., Sheng, Z., Liu, C., Yang, X., Liang, Y., Zhang, L., Liu, C., Kuang, X., Luo, S., You, Y., Zhang, X., 2019. Five-year observation of aerosol optical properties and its radiative effects to planetary boundary layer during air pollution episodes in North China: intercomparison of a plain site and a mountainous site in Beijing. *Sci. Total Environ.* 674, 140–158. <https://doi.org/10.1016/j.scitotenv.2019.03.418>.
- Zhong, J., Zhang, X., Dong, Y., Wang, Y., Liu, C., Wang, J., Zhang, Y., Che, H., 2018. Feedback effects of boundary-layer meteorological factors on cumulative explosive growth of PM_{2.5} during winter heavy pollution episodes in Beijing from 2013 to 2016. *Atmos. Chem. Phys.* 18, 247–258. <https://doi.org/10.5194/acp-18-247-2018>.
- Zhong, J., Zhang, X., Wang, Y., 2019a. Reflections on the threshold for PM_{2.5} explosive growth in the cumulative stage of winter heavy aerosol pollution episodes (HPEs) in Beijing. *Tellus B* 71, 1–7. <https://doi.org/10.1080/16000889.2018.1528134>.
- Zhong, J., Zhang, X., Wang, Y., Sun, J., Zhang, Y., Wang, J., Tan, K., Shen, X., Che, H., Zhang, L., Zhang, Z., Qi, X., Zhao, H., Ren, S., Li, Y., 2017. Relative contributions of boundary-layer meteorological factors to the explosive growth of PM_{2.5} during the red-alert heavy pollution episodes in Beijing in December 2016. *J. Meteorol. Res.* 31, 809–819. <https://doi.org/10.1007/s13351-017-7088-0>.
- Zhong, J., Zhang, X., Wang, Y., Wang, J., Shen, X., Zhang, H., Wang, T., Xie, Z., Liu, C., Zhang, H., Zhao, T., Sun, J., Fan, S., Gao, Z., Li, Y., Wang, L., 2019b. The two-way feedback mechanism between unfavorable meteorological conditions and cumulative aerosol pollution in various haze regions of China. *Atmos. Chem. Phys.* 19, 3287–3306. <https://doi.org/10.5194/acp-19-3287-2019>.